Article:
Pantopoulos, G, Manica, R, McArthur, AD et al. (2022) Particle shape trends across experimental cohesive and non-cohesive sediment gravity flow deposits: Implications for particle fractionation and discrimination of depositional settings. Sedimentology, 69 (4). pp. 1495-1518. ISSN: 0037-0746

https://doi.org/10.1111/sed.12960

DR. GEORGE PANTOPOULOS (Orcid ID : 0000-0002-3655-246X)

DR. ADAM DANIEL MCARTHUR (Orcid ID : 0000-0002-7245-9465)

Article type : Original Article

Particle shape trends across experimental cohesive and non-cohesive sediment gravity flow deposits: Implications for particle fractionation and discrimination of depositional settings

George Pantopoulos[1], Rafael Manica[2], Adam D. McArthur[3] and Juliano Kuchle[1]

[1]Instituto de Geociências, Universidade Federal do Rio Grande do Sul (UFRGS), Av. Bento Gonçalves 9500, CEP 91501-970 Porto Alegre, Brazil

[2]Instituto de Pesquisas Hidráulicas (IPH), Universidade Federal do Rio Grande do Sul (UFRGS), Av. Bento Gonçalves 9500, CEP 91501-970 Porto Alegre, Brazil

[3] School of Earth and Environment, University of Leeds, Leeds, LS2 9JT, UK

Corresponding author: George Pantopoulos (george_pantop@yahoo.gr)

Associate Editor – Fabrizio Felletti

Short Title – Particle shape trends-experimental gravity flows

ABSTRACT

Fractionation of particles in deep-water sediment gravity flows is an important factor in the resulting deposit and for discriminating sedimentary environments, but remains poorly understood. Quantitative characterization of particle shape was performed for more than ten-thousand particles of experimental gravity flow experiments (both of cohesive and non-cohesive nature) made using

coal and kaolin particles. Eleven particle shape parameters were calculated and their distribution and trends within the experimental basin were evaluated. Results indicate the existence of non-normal distributions and observable correlations between particle shape parameters. Shape parameters such as circularity and roundness are dominant controls on shape variation. Strong correlations exist between mean shape parameters and along-flow distance from the source for particles in non-cohesive flow experiments. Important differences were observed between shape parameter distributions of particles sampled at different areas within the experimental basin, which can be grouped based on their depositional setting (proximal or distal) using multivariate statistical analysis, especially for the non-cohesive flow experiments. A tendency for more elongated and irregularly-shaped particles at the more distal and marginal areas of the studied experimental basin was observed and validated by previous field studies in real-world deep-marine deposits. Besides, fractionation of particles is less-pronounced in cohesive flows compared with non-cohesive ones suggesting the soundness of discrimination of depositional settings based solely on particle shape characteristics is strongly dependent on parent flow characteristics. Yet, results highlight the potential of particle shape analysis in revealing spatial particle shape trends due to hydrodynamic fractionation and discriminating different depositional settings within submarine fans. This methodology may be applied to seafloor and subsurface samples to help identify the flow process and depositional environment.

Keywords: Clay content; flume tank; high density turbidity currents; organic matter; submarine fan; turbidites.

INTRODUCTION

Textural analysis is one of the most important aspects of sedimentary geology (Folk, 1974; Boggs, 2009). Together with composition, sediment texture (grain size, shape and fabric) is an essential part of sedimentary rock classification (Wentworth, 1922; Zingg, 1935; Krumbein, 1934; 1941; Krumbein & Sloss, 1951; Powers, 1953; Folk & Ward, 1957; Sneed & Folk, 1958; Illenberger, 1991). It can also provide important information regarding the sedimentary process and depositional conditions (Nichols, 2009). Especially for siliciclastic sedimentary rocks, textural data have been used since the inception of systematic sedimentary studies for assessing geological problems, such as determining the mode of transportation (e.g. Passega, 1957; 1964; Visher, 1969;

Sagoe & Visher, 1977) or verification of the depositional setting (e.g. Folk & Ward, 1957; Sneed & Folk, 1958; Friedman, 1961).

Characterization of grain shape in textural studies of sediments and sedimentary rocks has long been recognized as a vital element, especially for determining depositional environment and abrasion history of grains during transport and deposition (Wadell, 1932; Russel & Taylor, 1937; Krumbein, 1941). Taking advantage of the progress in computational methods, recent studies have focused on quantification of grain shape based on image analysis techniques (Tafesse *et al.*, 2013; Suzuki *et al.*, 2015; Campaña *et al.*, 2016; Takashimizu & Iiyoshi, 2016; Tunwal *et al.*, 2018; Fukuda & Naruse, 2020). Tunwal *et al.* (2018) introduced an image analysis procedure for quantifying various shape parameters previously proposed in the literature (Wadell, 1932; Riley, 1941; Orford & Whalley, 1983; Hyslip & Vallejo, 1997; Rao *et al.*, 2002; Blott & Pye, 2008; Roussillon *et al.*, 2009), to determine the textural maturity or depositional setting of sediments. However, to date, particle shape variation was mainly investigated in glacial, fluvial, beach, aeolian and coastal depositional settings, whereas deep-water sediments have received little attention (Marchand *et al.*, 2015; Bell *et al.*, 2018). Pyles *et al.* (2013) documented spatial fractionation of grains based on their shape and density, using soda-lime and zirconia-silicate glass particles in experimental gravity flows. Except for siliciclastic particles, several recent studies also documented hydrodynamic fractionation of organic material within sediment gravity flow deposits (McArthur *et al.*, 2016a; 2016b; 2017; Schnyder *et al.*, 2017).

To address the knowledge gap regarding grain shape variation within sediment gravity flow deposits and to test previous observations regarding fractionation of organic material within turbidites, the present study quantifies the shapes of particles from experimental gravity flows (composed of coal material) of both cohesive and non-cohesive nature, based on the procedure proposed by Tunwal *et al.* (2018). The main objectives of this work are: (i) to investigate the existence and nature of important particle shape parameter changes within the studied sediment gravity flow deposits (e.g. downstream changes in shape); (ii) to assess whether these changes can give information regarding depositional setting, in terms of simulated channel and lobe depositional settings; (iii) to check whether gravity flow parameters (clay content, concentration, etc.) affect particle shape distribution within the studied sediment gravity flow deposits; (iv) to verify whether the observed coal particle shape parameter distribution could have implications regarding organic matter distribution within deep-marine systems; and (v) to compare

experimental results to those of previous work from the outcropping Peïra Cava turbidite system in south-east France to investigate the validity of the study.

This study provides the first published and extensive dataset of quantitative shape parameters of particles from experimental sediment gravity flows, being simulations of both high-density turbidity currents and low strength cohesive debris flows (Talling *et al.*, 2012). The dataset and its processing results has implications for particle transport and distribution in deep-marine sedimentary systems. If successfully scaled up, as supported by a comparison with real-world examples, this work can provide a potential new method to constrain the depositional environment in subsurface studies based on grain shape, which can be integrated with other types of data such as seismic, well log, etc. This method can also provide insights regarding spatial changes in particle shape parameters with implications of particle shape variation for the quality of deep-marine clastic hydrocarbon reservoirs.

METHODS

Apparatus

The experiments were performed in a 2 m deep concrete and masonry tank including an inlet channel and a basin with sizes (length x width) 5 m x 2 m and 17 m x 7 m, respectively (Fig. 1). A fibreglass chute with parabolic section and a length of 4.8 m and a slope of 13.7˚ was inserted in the inlet channel, to replicate the typical cross-sectional shape of a canyon. At the end of the chute, a concrete transition zone was built to adjust the canyon topography with the flat basin.

A fibreglass reservoir with a 5000 l capacity, located 4 m above the tank was used to mix water and sediment. Two mixers were installed in the reservoir so to ensure homogeneity of the water–sediment mixture. The reservoir was connected to the inlet channel through a pipe and valve system instrumented with an electromagnetic flow-meter recording flow discharge at a 1 Hz frequency. In addition, a bypass pipe was installed to collect the sediment mixture just before the tank, in order to assess parameters such as grain size and variations in sediment concentration/mixing. A parabolic diffuser was placed at the end of the pipe to hydraulically adjust the mixture injected into the chute. At the end-wall of the basin, a draining system was

installed to drain the excess ambient water from the tank, thus keeping the water level constant during the experiments.

Sediment used

The flow mixture was composed of freshwater and two types of a sediment analogue, intended to reproduce non-cohesive and cohesive particles. Mineral coal (Cardiff type 205) with a density of 1.19 g/cm³ and a commercial grain size ranging from 1 to 350 μm was used as an analogue for non-cohesive particles. Coal particles used had a range of settling velocities from 0.0248 to 0.7116 cm/sec, measured in a Griffith tube. Mineral coal was sieved before use in order to assert the desired grain size range for each flow experiment. Optical assessment of initial particle shape for this type of mineral coal material was performed in previous studies (Manica, 2002) and showed the prevalence of particles having a sub-angular to sub-rounded shape (*sensu* Powers, 1953). Coal was used to represent non-cohesive particles and to help the comparison (scale) between small-scale experiments of turbidity currents and natural flows (Middleton, 1993; Manica, 2002; Castro, 2016). Kaolin, with a density of 2.6 g/cm³ and a commercial grain-size distribution ranging from nearly 0 to 60 μm was used as an analogue of fine, cohesive particles within the clay-rich flows (Baas *et al.*, 2014).

The particle size composition was roughly grouped in three classes of grain size distribution (Table 1): (i) fine-grained particles (F), representing clay to coarse silt (1–74 μm); (ii) medium-grained particles (M), containing very fine to fine sand, (74–174 μm); and (iii) coarse-grained particles (G), ranging from fine to medium sand (174–350 μm).

Experimental set up

Flow experiments started with the preparation of a 400 l mixture within the reservoir, and settling the water level in the experimental tank at 1.38 m, so to ensure that the fibreglass chute was submerged. Six glass-beakers were prepared to collect the injected mixture, through the bypass system. Three samples were collected prior to the experiment and three afterwards, to verify whether the bulk volumetric concentration was stable over time.

For all runs, the total amount of water–sediment mixture (total discharged volume) was the same and was discharged (injected) using a constant flow rate (Table 1). The discharge was controlled manually by an inlet valve. During the experiments, top-view images of the flow were

recorded every 10 seconds and discharge measurements were continuously acquired by the use of a data logger. After the total volume of sediment mixture was injected into the tank, the mixing inlet valve was closed. The tank was carefully drained after three hours to allow all grain-size classes to be deposited. In order to avoid any sediment remobilization, the total time needed to fully drain the tank was five days.

Seven different flow simulations were tested by combining different discharge rates (30, 40 and 50 l/min) and volumetric concentration (10, 20 and 26%), as detailed in Table 1. In particular, four experiments had 0% clay (clay-poor runs – F1E5, F1E7, F1E11 and F1E15) and three experiments had clay content ranging from 27 to 40% (clay-rich runs – F2E2, F2E3 and F2E4). Measured flow discharge was very consistent with target values, while the measured volumetric concentrations showed approximately 10% variation. The median grain-size (D50, determined using a laser diffractometer) also shows similar values for clay-free runs and was reduced (in comparison to clay-free flows) as clay was added to the mixture (Table 1).

Experimental flow types

Based on flow characteristics such as sediment concentration and clay content (Table 1) an approximation of experimental flow types was attempted also considering previous literature. Clay-poor flows simulated in the experiments can be theoretically classified as concentrated density flows, *sensu* Mulder & Alexander (2001) or high-density turbidity currents (Lowe, 1982). These types of flows are characterized by the presence of multiple grain support mechanisms and a two-layer flow structure. A basal dense flow layer is generated, in which turbulence, 'grain to grain' interactions, buoyancy and hindered settling can jointly act as main grain support mechanisms. At the top of the current, a high turbulence layer occurs, where the grains are supported by the ascendant component of turbulence (Middleton & Hampton, 1973). Deposition occurs by the settling of the grains along the flow path. However, once turbulence is suppressed and gravitational forces are reduced, the dense basal layer tends to deposit grains very quickly because the packed grains it carries can no longer be transported.

Clay-rich flows can be theoretically classified as low strength cohesive debris flows (*sensu* Talling *et al.*, 2012) or viscous high-density turbidity currents, close to the rheological limit between Newtonian and non-Newtonian flows (*sensu* Manica, 2012). In these types of flows, viscosity plays an important role at the base of the flow, but turbulence is not completely

suppressed as in a classic debris flow (Middleton & Hampton, 1973). During the experiments, all clay-rich flows exhibited Newtonian behaviour with limited influence of viscous forces. Clay-rich flows entering the channel were characterized by a decrease in concentration along their length due to deposition and dilution, thus indicating that these flows were not classic debris flows. Additionally, mass flow or cohesive freezing was not observed.

Grain shape parameters acquisition and statistical analysis

For detailed grain shape analysis, seven locations were selected across the tank basin, representing distinct proximal to distal depositional settings across a main longitudinal profile (Fig. 1). Sampling of these positions was repeated for all flow experiments. In addition, another three tank positions were sampled after two flow experiments: (i) an off-axis basin position (basin off-axis) along with a position close to the lateral basin margin (basin margin 1) for clay-poor F1E5 flow experiment (in order to have a basin cross-section particle shape trend); and (ii) |two lateral basin margin positions (basin margins 1 and 2) for clay-rich F2E4 flow experiment, in order to give a strike-orientated trend across the basin (Fig. 1). Also, sampling of sediment from the bypass system (before entering the tank) was performed for all flow experiments except one (F1E7, due to a problem in the bypass pipe), in order to conduct observations regarding initial particle shape.

Glass slides (Fig. 3) were prepared from 53 dry sediment samples across the above locations, using a wet mount approach (diluting the sample with distilled water), and studied using a Leica DM750 optical microscope equipped with a Leica MC170 digital camera, at a magnification of 100x and 200x (Leica Microsystems, Wetzlar, Germany). Particle microphotographs were acquired with a 1024 x 768 pixel resolution. Particle boundaries were drawn on the acquired microphotographs using graphic design software and extracted at a resolution of 300 dpi. The acquired boundaries were subsequently analyzed based on the image analysis procedure proposed by Tunwal *et al.* (2018) to quantify particle shape. Due to microscopic limitations, particle shape was determined until a minimum grain-size limit of 20 μm, using higher magnification (200x) for finer-grained samples. The number of measured particles per slide was in the range of 100 to 302, with a mean of 203 particles per slide. In total, shape parameters were extracted from 10044 particles (see also supplementary material).

During image analysis of microphotographs, eleven particle shape parameters were extracted (Table 2). Particle shape data processing was conducted in R software (R Core Team,

2021) using similar statistical analysis and rationale as in Tunwal *et al.* (2018) to make comparisons (Table 3). Pairwise correlations between studied particle shape parameters, as well as across-deposit correlations of mean shape parameters versus distance, were investigated using Pearson's r coefficient (Freedman *et al.*, 2007). Additionally, calculated shape parameters from all studied samples were tested for deviation from a normal (Gaussian) distribution, using a Shapiro–Wilk normality test (Shapiro & Wilk, 1965). Spatial variability of shape parameters distributions was visualized using boxplots. Mean shape parameters against known distance from the sediment's source were also plotted. These mean shape parameters were also interpolated using scatter plots. Principal component analysis (PCA), a multivariate statistical technique (Jolliffe, 2002), was implemented in order to investigate variation of shape in each flow dataset. This allowed the authors to investigate whether there were specific shape parameters that better controlled shape variation in each flow experiment.

As a measure for detecting significant differences between samples based on their locations and the distributions of their shape parameters, a Kruskal –Wallis statistical test (along with an additional *ad hoc* Dunn test) were used (Kruskal & Wallis, 1952; Dunn, 1964) following Tunwal *et al.* (2018). This test first checks whether a statistically significant difference exists for a particular shape parameter distribution between samples from one studied flow dataset. If a difference exists, then an additional test is performed (Dunn test), which compares all possible pairs of samples from each flow and indicates whether they exhibit a large difference in their particle shape distribution (or not). The test was performed with a 95% significance level.

An attempt to detect clusters of samples based on their shape parameters was made using hierarchical clustering techniques (Kaufman & Rousseeuw, 1990). Cluster analysis has been applied using Ward's method (Ward, 1963), separately for clay-poor and clay-rich flow datasets, using descriptive statistics of calculated shape parameters (mean, median, standard deviation, first and third quartile).

Flow upscaling

To investigate whether the experimental flows generated could be dynamically compared with natural flows, scale analysis was applied, using two reduced scale methodologies previously described for similar flow experiments (Pyles *et al.*, 2013; Baas *et al.*, 2014). Using both proposed methods, the upscaling of experimental results to reality based on observed parameters (for

example, for deposit geometries and dimensions, Fig. 2) was in good approximation compared with values reported in the literature for flow characteristics and deposits of natural turbidity flows. Details of flow upscaling results and methods applied can be found in Supplementary File 1.

RESULTS

Parameter correlations – normality testing

Pairwise correlations between studied particle shape parameters for all studied gravity flows (using Pearson's r coefficient), showed strong correlations between parameters such as circularity, aspect ratio, compactness and mod ratio (Fig. 4). Fractal dimension, roundness, angularity, solidity, irregularity and rectangularity exhibit weaker correlations with other parameters. On the contrary, convexity does not show significant correlations with other parameters (Fig. 4). Normality testing results indicate that for the majority of samples from all studied flows, observed shape parameters deviate from a normal distribution (Table 4).

Spatial variability of shape parameters distribution

Boxplots presenting the median as well as the interquartile range of calculated shape parameters for each flow experiment were also created for investigating along-flow (channel to distal basin), or cross-flow trends (Fig. 1). Examples of the boxplots are presented here as well as in Supplementary File 2.

Along-flow particle shape changes

From a visual inspection of the plots (Figs 5, 6 and Supplementary File 2), some trends in the observed parameters can be seen along the basin longitudinal profile, both for clay-poor and clay-rich flow experiments. In general, circularity (Figs 5 and 6), solidity, rectangularity, compactness and mod ratio values all tend to decrease down-flow (Supplementary File 2) from channel to distal basin settings especially for clay-poor experiments. On the contrary, increasing trends are observed for fractal dimension (Fig. 5C), aspect ratio and irregularity (Supplementary File 2, also for clay-poor flows). An irregular pattern can be seen for angularity values (Fig. 5D) with differences between clay-poor and clay-rich flows (Figs 5 and 6). No visible trends were observed

for roundness (Figs 5B and 6B) and convexity (Supplementary File 2) values between channel and distal basin settings (with the exception of a possible weak increasing trend for roundness in clay-poor flows, Fig. 5B).

Cross-flow particle shape changes

The deposit created by the clay-rich flow F2E4 was also investigated in three positions spanning a strike-orientated profile between the two margins of the tank, passing through a central basin area (Fig. 1). Observed parameter variation trends include a decrease in circularity, solidity, rectangularity, compactness and mod ratio towards the basin's margins (Fig. 8A and Supplementary File 2). On the contrary, a slight increase in aspect ratio, fractal dimension, angularity and convexity can be seen towards the margins, while no trend is observed for roundness and irregularity (Fig. 8 and Supplementary File 2).

Shape trends within the deposit created by the clay-poor F1E5 flow were also investigated in a basin oblique cross-section profile spanning three positions located in the central proximal basin, a basin off-axis area and a position located at the basin's margin (Fig. 1). Observed variations from proximal basin towards the basin's margin, include a slight decrease in circularity, compactness, mod ratio, solidity, convexity and rectangularity (Fig. 7A and Supplementary File 2), a slight increase in aspect ratio and irregularity, while no or irregular trends are observed for fractal dimension, angularity and roundness (Fig. 7 and Supplementary File 2).

Particle shape changes versus along-flow distance

The realization of flow experiments within a tank basin and the sampling of known positions within a central longitudinal profile allowed the correlation of mean shape parameters against known distance from sediment's source. Using Pearson's r coefficient, distinct correlation trends and differences between flows were observed. Clay-poor flows exhibit strong correlations of shape parameters vs. distance (Table 5). In particular, a statistically significant downflow decrease is observed in all clay-poor flows for mean values of circularity, compactness and mod ratio. Additionally, in the majority of clay-poor flows a statistically significant decrease is observed for solidity and rectangularity, and a downflow increase can be seen for aspect ratio, irregularity and fractal dimension (Table 5). Roundness exhibits non-significant increasing trends for clay-poor flows while angularity shows contrasting trends: an increasing one (for F1E5 and F1E7 flows) or

very weak non-significant negative one (for F1E11 and F1E15 flows). Convexity does not exhibit particular downflow trends in the majority of studied clay-poor flows, exhibiting only a significant downflow increasing trend for flow F1E7 (Table 5).

On the contrary, clay-rich flows do not exhibit statistically significant mean shape versus distance correlations for the majority of studied particle shape parameters (Table 5). Only two statistically significant trends were seen, an increasing one for aspect ratio (only for the F2E2 experiment) and a decreasing one for angularity (only for the F2E3 experiment). However, similar non-significant trends can be seen in all clay-rich flows for circularity, compactness, mod ratio and aspect ratio (Table 5).

Principal component analysis (PCA)

Results of this multivariate analysis (Table 6) indicate that for all experiments there are two principal components that express more than 60% of shape variation (Table 6). The first main component is better correlated with circularity (in most cases) and mod ratio. The second component is better correlated with roundness and fractal dimension (Table 6).

Mean shape parameters scatter plots

Scatter plots of mean shape parameters from all samples were created, in order to investigate possible trends between samples from different sampling positions. Selected parameters for plotting were based on previous analysis (for example PCA and shape versus distance correlations). Thus, parameters such as circularity, roundness, fractal dimension and solidity were selected because they seem to control a large portion of shape parameter variation (Table 6) and exhibit strong downflow distance correlations (for example, circularity and solidity).

Plotting of mean circularity versus mean roundness (Fig. 9) exhibits a trend for more distal samples (distal basin and basin 3 positions, Fig. 1) to have lower circularity and higher roundness values, especially for clay-poor flow samples (Fig. 9A), while clay-rich samples do not show a clear trend (Fig. 9B). Circularity versus fractal dimension plot shows a similar trend for samples of clay-poor flows, with a clearer distinction between proximally-located and distally-located samples (Fig. 10A). Again, clay-rich flow samples do not exhibit a clear trend (Fig. 10B). Plots of circularity versus solidity exhibit an opposite trend with distally-located samples having lower

values for both parameters, but samples of clay-poor flows can be more easily separated based on their location compared with those of clay-rich flows (Fig. 11).

In general, samples from clay-poor flows seem to exhibit a clearer trend in regard to their location in all shape parameter scatter plots, with the exception of samples belonging to the transitional area (between the channel and the proximal basin), which show an irregular behaviour. Plotting of mean shape parameters for samples taken from the bypass system (before entering the tank) usually exhibits values situated at the medial range of those observed between different sampling areas of the tank (especially for clay-poor flows), with an exception for roundness which seems to be generally lower for coal particles from bypass samples (Figs 9 to 11).

Kruskal–Wallis (and *ad hoc* Dunn) testing

Results of this statistical test indicate that sample pairs from clay-poor flows exhibit a larger number of differences between sample locations (Supplementary File 2): From a total of 924 comparisons, 209 (around 22.6%) exhibited an important difference. In particular important differences were detected between sample pairs such as: basin 1/2/3–distal basin, proximal–distal basin, channel–distal basin, channel–basin 3 and transition–distal basin (Supplementary File 2). Parameters that showed larger differences between samples were angularity, circularity, rectangularity, compactness, solidity and mod ratio. On the contrary, important differences in roundness were not detected between all tested sample pairs (Supplementary File 2).

Regarding sample pairings from clay-rich flows, a smaller number of differences between sample locations was detected (Supplementary File 2): From a total of 693 comparisons, 104 (approximately 15%) exhibited important differences. Those differences were mainly detected between sample pairs such as: channel–distal basin and basin 1/2/3–distal basin (Supplementary File 2). Parameters that showed larger differences between samples were angularity, rectangularity, solidity and mod ratio. Important differences in roundness as well as in irregularity were not found between tested samples (Supplementary File 2).

Hierarchical clustering

The clustering approach for clay-poor flows was able to separate two main clusters characterized by distally-located and proximally-located samples respectively (Fig. 12). The main distal cluster is composed of two sub-clusters, one dominated by distal basin and basin margin samples (five out

of seven, around 71.5%), and another dominated by basin samples (six out of eight, 75%) mainly located at the more distal parts (basin 2 and 3 samples). The main proximal cluster is also composed of two sub-clusters, a smaller one dominated of channel-located samples (two out of three, 66.6%) and a larger one mainly composed of channel, transition and proximal basin samples (seven out of 12, around 58.3%) and some basin samples located at the more proximal parts (mainly basin 1 samples). It must be noted that samples originating from the channel-basin transitional area, showed an irregular behaviour, appearing in both proximal and distal main clusters (Fig. 12).

The clustering procedure for clay-rich flow samples does not indicate the presence of characteristic sample clusters based on their location. Although some sub-clusters are seen, mainly composed by distally-located basin and distal basin/basin margin samples (Fig. 13), these are smaller and do not belong to the main cluster, being mixed with more proximally-dominated sub-clusters.

DISCUSSION

Shape parameters correlation and distribution

Pearson's r coefficient between calculated shape parameters revealed strong correlations between variables such as circularity, compactness, aspect ratio and mod ratio. This was also observed in the study of Tunwal *et al.* (2018) and is attributed to the definition of these shape parameters (Table 2), which is similar and depends on circle-related attributes of the particles (especially for circularity, compactness and mod ratio). More sophisticated shape parameters such as roundness, angularity and fractal dimension showed moderate to very weak correlations in our study. Roundness seems to not have strong correlations with other parameters and only shows some weak correlations with compactness and aspect ratio (Fig. 4). Angularity shows some moderate to weak correlations with fractal dimension, rectangularity and solidity (Fig. 4). Fractal dimension is moderately-correlated with solidity and weakly-correlated with rectangularity, irregularity and angularity (Fig. 4). These correlations between fractal dimension, angularity and solidity were also observed by Tunwal *et al.* (2018) in their study of grain shapes from glacial, fluvial, beach and aeolian depositional environments, but were more pronounced. These authors attributed the

observed correlations to the context of 'textural maturity' (Folk, 1951) of grains as they get more 'rounded' or 'smoothed' shapes, passing from glacial to aeolian environments. Results of the present study also observed the above correlations but with a less pronounced effect: a positive weak correlation seems to exist between fractal dimension and angularity, and a moderate negative correlation between fractal dimension and solidity (Fig. 4). This less-pronounced effect is attributed either to image resolution biases during image analysis or to the fact that the compared shape attributes are not coming from grains that had a significantly different abrasion history (as for those of Tunwal *et al.* 2018), but only experienced hydraulic segregation within an experimental flow.

Another similar finding of this study compared with the work of Tunwal *et al.* (2018) is that the majority of calculated shape parameters are not characterized by a normal (Gaussian) distribution, irrespective of sample and position within the experimental basin. The latter observation could be related with the existence of skewed distributions of shape parameters in several samples as it can be seen from the observed shapes of boxplots (Figs 5 and 6).

Downflow or along-flow shape parameter trends

Boxplot and mean shape versus distance analysis indicates that several along-flow shape parameter trends exist in the studied datasets (Figs 5, 6 and 9 to 11). These trends tend to be stronger in the studied clay-poor, non-cohesive flows. Especially for simple shape parameters such as circularity and aspect ratio an opposite trend of downcurrent decrease and increase respectively is observed. This observation indicates the downcurrent occurrence of more platy and elongated particles, especially at the distal basin area.

Regarding more sophisticated shape parameters, there are also observable trends such as the downcurrent decrease in solidity, and increase in fractal dimension and irregularity which indicate the downflow occurrence of more concave and 'rough-shaped' particles. Also, angularity exhibits a downcurrent increase at least in clay-poor flow experiment F1E7. These trends are in contrast with observations made by Tunwal *et al.* (2018), who proposed that increasing textural maturity of grains from glacial to aeolian settings is reflected by increasing solidity and decreasing angularity and fractal dimension trends. This contrast can be attributed to measurement biases due to the relatively low image resolution used in the present study, but may also be due to the

different nature of sedimentation in the case of subaqueous flow experiments and also to the different composition of sediment used (mineral coal).

Which shape parameters best capture grain shape variations in sediment gravity flows?

In their study, Tunwal *et al.* (2018) observed that important shape parameters for determining 'textural maturity' of a sediment sample are mainly more sophisticated (needing advanced calculations for their assessment) parameters such as angularity and fractal dimension. On the contrary, simpler to calculate, traditionally-used parameters such as circularity or aspect ratio were not found as important in determining textural maturity, in agreement with Campana *et al.* (2016). According to Tunwal *et al.* (2018) a texturally 'mature' sediment sample is mainly characterized by grains with lower angularity and fractal dimension values compared with an 'immature' sediment.

Results of this study, however, indicate that simple shape parameters are still important in capturing grain shape variation, at least for subaqueous sediment gravity flow experiments. In particular, an important part of grain shape variation in the studied flow experiments seems to be characterized by differences in circularity, as shown by PCA analysis and also by strong downcurrent trends in this shape parameter (Table 5). On the other hand, regarding more advanced shape parameters, it seems that indeed fractal dimension also plays an important role in capturing the observed grain shape variation, in agreement with Tunwal *et al.* (2018). However, observed fractal dimension trends of this study tend to have a different behaviour, exhibiting a downcurrent increase, which is probably attributed to measurement bias due to lower image resolution used. The PCA analysis also highlighted the important role of roundness, which does not seem to exhibit important differences between samples, as the Kruskal–Wallis test indicated, but seems to capture an important part of grain shape variation and also seems to have a statistically significant downcurrent increasing trend, especially for F1E7 clay-poor flow experiment (Table 5).

Possible process-product controls on observed particle shape trends

Initial particle shape

It is possible that the observed particle shape variation could be affected by the initial shape of the coal particles used for the realization of flow experiments. However, efforts have been made to avoid these effects, firstly by removing the very fine ('dust') particles of the mineral coal used

(which are usually characterized by irregular shapes due to milling processing of the coal) and also by visually checking the particles before the experiments. Previous analysis and use of this type of mineral coal material within sediment gravity flow experiments (Manica, 2002; Castro, 2016) showed that it is mainly characterized by sub-angular to sub-rounded particles which have a very good hydrodynamic behaviour for simulating turbidity flows at smaller scales. Secondly, an effort was also made in quantitatively analyzing particle shape for samples taken from the bypass system (before entering the tank). The extracted mean shape values were situated at the medial range of those observed between different sampling areas of the tank (Figs 9 to 11), implying the existence of irregularly-shaped and platy particles within the original sediment mixture inserted in the tank. The prevalence of these more irregularly-shaped, platy particles within the distal and marginal areas of studied experimental deposits, indicates possible effects of studied experimental flows, which probably segregated the particles incorporated within them based on their shape: irregularly shaped particles were probably much easier to keep in suspension which would explain their observed increasing trend as a result of along-flow hydraulic fractionation in a similar manner to previous studies (Pyles *et al*., 2013).

However, coal particles from bypass samples are generally less-rounded (Figs 9, 10 and 11), implying a slight shape modification of the initial coal particles along the flow, also implied by the weak increasing downflow trends in roundness values within the experimental basin. Nevertheless, along-flow shape modifications do not seem to play an important role in controlling shape variation within the studied experimental deposits when compared with hydraulic fractionation of grains.

Image resolution

Due to lower image resolution in comparison with the microphotographs analyzed by Tunwal *et al.* (2018) and the finer particle sizes incorporated in our study, measurement bias due to image resolution is possible to be present and it is probably reflected in the more sensitive shape parameters like angularity and convexity for example, which do not correlate well with other shape parameters and are not characterized by particular downcurrent trends. The latter bias is also probably validated by the downcurrent increase in fractal dimension, a parameter which reflects grain boundary roughness: a smaller particle would be characterized by a rougher, more pixellated boundary in lower image resolution. However, the observation of well-documented along-flow

trends in aspect ratio and circularity, coupled with a slight increase in roundness (which again is not so pronounced probably due to possible image resolution bias) indicate the actual fractionation of the particles within the studied flows based on shape. Further analysis with very high resolution images of higher magnification will indicate whether downcurrent trends in angularity, convexity and fractal dimension are also present in deposits of sediment gravity flows. However, results from the present study are promising, showing that even simpler image analysis using lower resolution images is capable of recognizing downcurrent shape trends within sediment gravity flow deposits and can classify them according to their depositional setting.

Flow properties

The observed differences in shape parameter trends, especially between non-cohesive and cohesive flow experiments, imply that flow properties affected particle shape variation. From results presented (Table 5) is clear that clay-poor experimental flows characterized by non-presence of clay content, are showing statistically significant along-flow trends in grain shape variation.

The latter along-flow trends are less pronounced (or non-existent) in the studied cohesive clay-rich flows. This is attributed to the presence of significant clay content, which probably led to the creation of flocs and gels (Winterwerp & van Kesteren, 2004) within the flows which increased flow viscosity and significantly suppressed flow turbulence (Baas & Best, 2002).

Except for clay content, flow concentration seems also to play a role in the observed downcurrent shape trends. Clay-poor flow F1E7, characterized by the lower concentration (12.5%) in comparison to all other flow experiments, exhibits statistically significant downcurrent trends in almost all studied shape parameters (Table 5). Lower concentration flows are generally characterized by the prevalence of turbulence as a main grain support mechanism.

The above observations agree with previous studies that showed the effects of clay content and flow concentration to the properties and deposits of sediment gravity flows. In a recent study Baker *et al.* (2017) clearly showed that cohesive experimental flows containing kaolin are characterized by shorter runout distances and lower head velocities and mobility compared with clay-free, non-cohesive flows of silica flour. Thus, it is possible for clay-free, non-cohesive flows (similar to those of the present study) to be highly turbulent and extremely mobile in order to

better fractionate the particles within them. In contrast, cohesive flows containing kaolin will be characterized by decreased mobility and frictional forces which will reduce particle support in the flow and thus prevent particle fractionation.

Comparison with an ancient turbidite system

The results of this study may be compared with the organic matter composition of ancient turbidites that crop out in the Peïra Cava Basin, south-east France (McArthur *et al.,* 2016b). Here, the deposits from individual turbidity currents can be tracked across the preserved basin fill, giving a proximal to distal trend (Amy *et al.*, 2007) and a framework in which to characterize downcurrent and across basin trends in the composition and dimensions of organic particles. A general trend of particles becoming smaller, elongated and less spherical was observed (McArthur *et al.*, 2016b; Fig. 14). This compares well with findings of the present study, which also demonstrates decreasing trends in circularity and increasing aspect ratio values from channel to distal basin settings.

Additionally, flow upscaling analysis (Suppl. File 1) based on two previous methodologies (Pyles *et al*., 2013; Baas *et al*., 2014) revealed that experimental flow and deposit parameters (flow properties, deposit dimensions and grain-size characteristics) are in good approximation compared with values reported in the literature for flow characteristics and deposits of natural turbidity currents (Talling *et al*., 2013). More particularly, upscaling values for mean flow velocity at the range of 6 m/sec, calculated flow thickness of ≈ 90 m, Froude and Reynolds numbers of approximately 0.35 and 10^8 respectively, lobe widths of ≈ 4400 m and lobe thicknesses of around 28 m are all within range of values observed in real-world turbidity flows and deposits. Thus, the above findings provide confidence that the experimental flow data are replicating natural flows and support the assumption that particle shape variations observed in the present experimental study could correspond to the ones that can be found within natural deep marine sedimentary systems.

Discrimination of depositional environment

Tunwal *et al.* (2018) proposed that quantitative grain shape analysis can provide reliable information regarding the textural maturity of a sediment sample, but recommended caution

regarding attempts to distinguish sedimentary environment based on grain shape alone. On the contrary, Suzuki *et al.* (2015) managed to distinguish siliciclastic grains from different depositional environments based on elliptical Fourier descriptor analysis. Based on an alternative type of Fourier descriptor analysis, Fukuda & Naruse (2020) were also able to detect mud clast shape differences in a single flow event, associated with different depositional facies and transport processes rather than with along-flow distance.

Due to the origin of the grain shape data used in this study (flow experiments) it was not considered that the observed grain shape trends and variation expresses respective trends in textural maturity, but are rather related to deposition closely controlled by the characteristics of the created gravity flows and their evolution within the experimental basin. Grain shape variation based on depositional setting is indicated by previous results from statistical analysis of calculated grain shape parameters. Kruskal–Wallis statistical testing indicated important differences between grain shape distributions in different parts of the tank basin. Hierarchical clustering analysis based on descriptive statistics of all of the calculated grain shape parameters, as well as bivariate plotting of mean grain shape, indicated that especially for the case of non-cohesive clay-poor flows, it is possible to differentiate between depositional settings within a submarine fan environment. Moreover, grains from the distal and marginal parts of the experimental deposits are characterized by different grain shape characteristics, when compared with those from more proximal deposits (channel and proximal basin settings). Clustering techniques grouped together non-cohesive flow samples from distal basin/basin margin, basin and channel/proximal basin settings respectively (Fig. 12). However, in the case of cohesive flows, this discrimination is not straightforward, probably due to the presence of fine-grained matrix and flocculation which prevented possible flow fractionation of grains.

Channel to basin transitional area

It is important to note that the above particle shape analysis shows that particles originating from the transitional area between channel and proximal basin settings, exhibit an erratic behaviour both in clustering dendrogram and mean grain shape biplots, appearing not to form distinct clusters or to get plotted close to the more proximal samples (Figs 9 to 12). This observation could be related to the nature of flow modifications in this part of the basin. It is very possible that intense flow transformations that are occurring in this area (flow deceleration and expansion) are severely

affecting particle shape distribution. Similarly, in the outcrop analogue, the base of slope sediments of the Peïra Cava Basin showed the poorest sorting of organic particles (McArthur *et al.*, 2016b).

Practical applications

Results from the previous particle shape analysis could offer general guidance regarding particle shape differentiation between different depositional settings of deep-marine systems (Fig. 15) solely based on quantitative particle shape data (possibly extracted from cores or thin sections). Observed particle shape differentiation within the studied experimental basin, implies hydrodynamic fractionation of the studied coal particles based on shape. The latter could also have implications regarding transport and distribution of organic matter within deep-marine systems, highlighting the usefulness and application of proposed methodologies such as palynofacies analysis (McArthur *et al.*, 2016a; 2016b; 2017) towards discrimination of deep-marine depositional environments. However, all available data (sedimentological, petrophysical, geophysical, etc.) should be integrated to make the most robust interpretation of the depositional environment.

Another observation of the present study regarding the prevalence of more elongated and irregularly-shaped particles at the distal and marginal areas of the created experimental deposits could also have implications for the evaluation of reservoir quality in deep-marine hydrocarbon reservoirs or carbon capture and storage sites. The prevalence of such types of particles at the distal and marginal areas of deep-marine deposits could lead to poorer reservoir qualities at these areas, as shown in recent field studies (Bell *et al.*, 2018).

CONCLUSIONS

Detailed shape analysis of particles from large-scale cohesive and non-cohesive experimental gravity flows shows that quantitative shape characterization holds potential in revealing possible hydrodynamic fractionation of particles. Particle morphology can also be used in evaluating the depositional setting within an experimental basin. Eleven studied shape parameters (of both simple and more advanced nature) are characterized by variable non-normal distributions, exhibiting

observable correlations between one another and trends between different sampling positions within a basin.

Shape variation can be likely captured by advanced shape parameters such as fractal dimension and roundness, but simpler parameters such as circularity also play an important role in capturing shape variation. Statistically significant trends were observed between mean shape parameters and along-flow distance from the source of sediment for the studied non-cohesive clay-poor flow experiments. These trends are absent or non-statistically significant in the studied cohesive clay-rich flows. Statistical testing revealed important differences in shape parameter distribution between different sampling positions. Scatter plot and cluster analysis indicate that it is possible to differentiate samples between different areas of the experimental basin and managed to group proximally-originated or distally-originated samples together, but only in the case of clay-poor, non-cohesive flow experiments. Generally, in the more distal and marginal parts of the studied experimental deposits more platy, elongated and irregularly-shaped particles are prevailing, characterized by decreased circularity and aspect ratio values compared with the more proximal and central parts of the deposits. These results indicate that the sedimentary processes involved in the transport of particles through an experimental basin by sediment gravity flows are at least partially responsible for the variation in depositional products.

The above observations, which simulated both high-density turbidity currents and low strength cohesive debris flows, are validated by previous field studies in real-world turbidite systems and highlight the potential of grain shape analysis towards discrimination of different depositional settings within sediment gravity flow deposits. Although caution is advised when applying this method to cohesive flows, where this discrimination is not always feasible and strongly depends on parent flow characteristics such as clay content for example. When carefully applied, this method can provide insights regarding spatial changes in particle shape parameters, which may be used to identify deep-marine architectural elements and assess the quality of clastic hydrocarbon reservoirs.

ACKNOWLEDGEMENTS

The authors gratefully acknowledge Petrobras (Petróleo Brasileiro S.A.) and its former research coordinator Marco A.S. Moraes for the support in the implementation of this research at Nucleo de Estudos de Correntes de Densidade (NECOD), Instituto de Pesquisas Hidráulicas (IPH), UFRGS. Mohit Tunwal (Penn State University) is also acknowledged for kindly providing shape analysis code along with advice for its use. Luiz Fernando De Ros (UFRGS) and Paulo Paraizo (Petrobras) are thanked for providing insightful discussions and suggestions. We would also like to thank Ian Kane, Fabrizio Felletti and Elaine Richardson for editorial handling. Mattia Marini and two anonymous reviewers provided constructive comments and criticisms which improved an early version of the manuscript.

DATA AVAILABILITY STATEMENT

Data available on request from the authors.

REFERENCES

Amy, L.A., Kneller, B.C. and **McCaffrey, W.D.** (2007) Facies architecture of the Grès de Peïra Cava, SE France: Landward stacking patterns in ponded turbiditic basins. *J. Geol. Soc.*, **164**, 143-162.

Baas, J.H. and **Best, J.L.** (2002) Turbulence modulation in clay-rich sediment-laden flows and some implications for sediment deposition. *J. Sed. Res.*, **72**, 336-340.

Baas, J.H., Manica, R., Puhl, E., Verhagen, I. and **Borges, A.L.O.** (2014) Processes and products of turbidity currents entering soft muddy substrates. *Geology*, **42**, 371-374.

Baker, M.L., Baas, J.H., Malarkey, J., Jacinto, R.S., Craig, M.J., Kane, I.A. and **Barker, S.** (2017) The effect of clay type on the properties of cohesive sediment gravity flows and their deposits. *J. Sed. Res.*, **87**, 1176–1195.

Bell, D., Kane, I.A., Ponten, A.S.M., Flint, S.S., Hodgson, D.M. and **Barrett, B.J.** (2018) Spatial variability in depositional reservoir quality of deep-water channel-fill and lobe deposits. *Mar. Petrol. Geol.*, **98**. 97-115.

Blott, P.J. and **Pye, K.** (2008) Particle shape: a review and new methods of characterization and classification. *Sedimentology*, **55**, 31-63.

Boggs, S. Jr. (2009) *Petrology of Sedimentary Rocks*. Second Edition, Cambridge University Press, 600 p.

Campaña, I., Benito-Calvo, A., Pérez-González, A., Bermúdez de Castro, J.M. and **Carbonell, E.** (2016) Assessing automated image analysis of sand grain shape to identify sedimentary facies, Gran Dolina archaeological site (Burgos, Spain). *Sed. Geol.*, **346**, 72-83.

Castro, C. (2016) *Propriedades reológicas de misturas utilizadas em simulaçâo física de correntes de turbidez*. MSc Thesis, Instituto de Pesquisas Hidráulicas, Universidade Federal do Rio Grande do Sul (UFRGS), Porto Alegre, Brazil.

Dunn, O.J. (1964) Multiple comparisons using rank sums. *Technometrics*, **6**, 241-252.

Folk, R.L. (1951) Stages of textural maturity in sedimentary rocks. *J. Sed. Petrol.*, **21**, 127-130.

Folk, R.L. (1974) *Petrology of Sedimentary Rocks*. Hemphill Publishing Co., Austin, TX, 182 pp.

Folk, R.L. and **Ward, W.C.** (1957) Brazos river bar: a study in the significance of grain size parameters. *J. Sed. Petrol.*, **27**, 3-26.

Freedman, D., Pisani, R., and **Purves, R.** (2007) *Statistics* (4th Edition). W. W. Norton & Company, New York, 697 pp.

Friedman, G.M. (1961) Distinction between dune, beach, and river sands from their textural characteristics. *J. Sed. Petrol.*, **31**, 514-529.

Fukuda, S. and **Naruse, H.** (2020) Shape difference of mud clasts depending on depositional facies: application of newly modified elliptic Fourier analysis to hybrid event beds. *J. Sed. Res.*, **90**, 1410-1435.

Hyslip, J.P. and **Vallejo, L.E.** (1997) Fractal analysis of the roughness and size distribution of granular materials. *Eng. Geol.*, **48**, 231-244.

Illenberger, W.K. (1991) Pebble shape (and size?). *J. Sed. Petrol.*, **61**, 756-767.

Jolliffe, I.T. (2002) *Principal Component Analysis* (2nd Edition). Springer, 405 pp.

Kaufman, L. and **Rousseeuw, P.J.** (1990) *Finding Groups in Data: An Introduction to Cluster Analysis* (1st Edition). John Wiley, New York, 342 pp.

Krumbein, W.C. (1934) Size frequency distributions of sediments. *J. Sed. Petrol.*, **4**, 65-77.

Krumbein, W.C. (1941) Measurement and geological significance of shape and roundness of sedimentary particles. *J. Sed. Petrol.*, **11**, 64-72.

Krumbein, W.C. and **Sloss, L.L.** (1951) *Stratigraphy and Sedimentation*. Freeman, San Francisco, 497 pp.

Kruskal, W.H. and **Wallis, W.A.** (1952) Use of ranks in one-criterion variance analysis. *J. Am. Stat. Assoc.*, **47**, 583-621.

Lowe, D.R. (1982) Sediment gravity flows: II. Depositional models with special reference to the deposits of high-density turbidity currents. *J. Sed. Petrol.*, **52**, 279-297.

Manica, R. (2002) *Modelagem física de correntes de densidade não conservativas em canal tridimensional de geometria simplificada*. MSc Thesis, Instituto de Pesquisas Hidráulicas, Universidade Federal do Rio Grande do Sul (UFRGS), Porto Alegre, Brazil.

Manica, R. (2012) Sediment Gravity Flows: Study Based on Experimental Simulations. In: *Hydrodynamics-Natural Water Bodies*, pp. 263-286. InTech Publ.

Marchand, A.M.E., Apps, G., Li, W. and **Rotzien, J.R.** (2015) Depositional processes and impact on reservoir quality in deepwater Paleogene reservoirs, US Gulf of Mexico. *AAPG Bull.*, **99**, 1635-1648.

McArthur, A.D., Kneller, B.C., Souza, P.A. and **Kuchle, J.** (2016a) Characterization of deep-marine channel-levee complex architecture with palynofacies: An outcrop example from the Rosario Formation, Baja California, Mexico. *Mar. Petrol. Geol.*, **73**, 157-173.

McArthur, A.D., Kneller, B.C., Wakefield, M.I., Souza, P.A. and **Kuchle, J.** (2016b) Palynofacies classification of the depositional elements of confined turbidite systems: Examples from the Gres d'Annot, SE France. *Mar. Petrol. Geol.*, **77**, 1254-1273.

McArthur, A.D., Gamberi, F., Kneller, B.C., Wakefield, M.I., Souza, P.A. and **Kuchle, J.** (2017) Palynofacies classification of submarine fan depositional environments: Outcrop examples from the Marnoso-Arenacea Formation, Italy. *Mar. Petrol. Geol.*, **88**, 181-199.

Middleton, G.V. (1993) Sediment deposition from turbidity currents. *Annu. Rev. Earth Planet. Sci.*, **21**, 89-114.

Middleton, G.V. and **Hampton, M.A.** (1973) Sediment gravity flows: mechanics of flow and deposition. In: *Turbidity and Deep-Water Sedimentation,* pp. 1-38. SEPM, Pacific Section, Short Course Lecture Notes.

Mulder, T. and **Alexander, J.** (2001) The physical character of subaqueous sedimentary density flows and their deposits. *Sedimentology*, **48**, 269-299.

Nichols, G. (2009) *Sedimentology and Stratigraphy*. Second Edition, West Sussex, John Wiley & Sons Ltd, 419 p.

Orford, J.D. and **Whalley, W.B.** (1983) The use of the fractal dimension to quantify the morphology of irregular-shaped particles. *Sedimentology*, **30**, 655-668.

Passega, R. (1957) Texture as characteristic of clastic deposition. *AAPG Bull.*, **41**, 1952-1984.

Passega, R. (1964) Grain size representation by CM patterns as a geological tool. *J. Sed. Petrol.*, **34**, 830-847.

Powers, M.C. (1953) A new roundness scale for sedimentary particles. *J. Sed. Petrol.*, **23**, 117-119.

Pyles, D.R, Straub, K.M. and **Stammer, J.G.** (2013) Spatial variations in the composition of turbidites due to hydrodynamic fractionation. *Geophys. Res. Lett.*, **40**, 3919-3923.

R Core Team (2021) *R: A language and Environment for Statistical Computing*. R Foundation for Statistical Computing, Vienna, Austria. Available at: https://www.R-project.org/.

Rao, C., Tutumluer, E. and **Kim, I.T.** (2002) Quantification of coarse aggregate angularity based on image analysis. *Transp. Res. Record: J. Transport. Res. Board*, **1787**, 117-124.

Riley, N.A. (1941) Projection sphericity. *J. Sed. Petrol.*, **11**, 94-97.

Roussillon, T., Piegay, H., Sivignon, I., Tougne, L. and **Lavigne, F.** (2009) Automatic computation of pebble roundness using digital imagery and discrete geometry. *Comput. Geosci.*, **35**, 1992-2000.

Russell, R.D. and **Taylor, R.E.** (1937) Roundness and shape of Mississippi River sands. *J. Geol.*, **45**, 225-267.

Sagoe, K.O. and **Visher, G.S.** (1977) Population breaks in grain-size distributions of sand: a theoretical model. *J. Sed. Petrol.,* **47**, 285-310.

Schnyder, J., Stetten, E., Baudin, F., Pruski, A.M. and **Martinez, P.** (2017) Palynofacies reveal fresh terrestrial organic matter inputs in the terminal lobes of the Congo deep-sea fan. *Deep-Sea Res. Part II*, **142**, 91-108.

Shapiro, S.S. and **Wilk, M.B.** (1965) An analysis of variance test for normality (complete samples). *Biometrika*, **52**, 591-611

Sneed, E.D. and **Folk, R.L.** (1958) Pebbles in the lower Colorado River, Texas, a study in particle morphogenesis. *J. Geol.*, **66**, 114-150.

Suzuki, K., Fujiwara, H. and **Ohta, T.** (2015) The evaluation of macroscopic and microscopic textures of sand grains using elliptic Fourier and principal component analysis: implications for the discrimination of sedimentary environments. *Sedimentology*, **62**, 1184-1197.

Tafesse, S., Robison Fernlund, J.M., Sun, W. and **Bergholm, F.** (2013) Evaluation of image analysis methods used for quantification of particle angularity. *Sedimentology*, **60**, 1100-1110.

Takashimizu, Y. and **Iiyoshi, M.** (2016) New parameter of roundness R: circularity corrected by aspect ratio. Prog. *Earth Planet. Sci.*, **3**, 1-16.

Talling, P.J., Masson, D.G., Sumner, E.J. and **Malgesini, G.** (2012) Subaqueous sediment density flows: depositional processes and deposit types. *Sedimentology*, **59**, 1937-2003.

Talling, P.J., **Paull, C.K.** and **Piper, D.J.W.** (2013) How are subaqueous sediment density flows triggered, what is their internal structure and how does it evolve? Direct observations from monitoring of active flows. *Ear.-Sci. Rev.*, **125**, 244-287.

Tunwal, M., Mulchrone, K.F. and **Meere, P.A.** (2018) Quantitative characterization of grain shape: Implications for textural maturity analysis and discrimination between depositional environments. *Sedimentology*, **65**, 1761-1776.

Visher, G.S. (1969) Grain size distributions and depositional processes. *J. Sed. Petrol.,* **39**, 1074-1106.

Wadell, H. (1932) Volume, shape, and roundness of rock particles. *J. Geol.*, **40**, 443-451.

Ward, J.H. (1963) Hierarchical grouping to optimize an objective function. *J. Am. Stat. Assoc.*, **58**, 236-244.

Wentworth, C.K. (1922) A scale of grade and class terms for clastic sediments. *J. Geol.*, **30**, 377-392.

Winterwerp, J.C. and **Van Kesteren, W.G.M.** (2004) Introduction to the physics of cohesive sediment in the marine environment. *Dev. Sedimentol.*, **56**, 576 pp.

Zingg, T. (1935) Beiträge zur Schotteranalyse. *Schweiz. Mineral. Petrog. Mitt.*, **15**, 39-140.

FIGURE CAPTIONS

Figure 1: Experimental tank facility sketch illustrating positions of studied samples and studied trend trajectories. Basin 1, 2 and 3 positions represent different positions within the central (axial) area of the tank.

Figure 2: Photographs of deposits geometries after the end of the studied experimental flows. (A) to (D) Clay-poor flows; F1E5 (A), F1E7 (B), F1E11 (C) and F1E15 (D). (E) to (G) Clay- rich flows; F2E2 (E), F2E3 (F) and F2E4 (G).

Figure 3: Examples of sample photomicrographs which were analyzed for particle shape parameters. (A) to (D) Clay-poor samples from; channel (A), proximal basin (B), basin 1 (C) and distal basin (D) positions (see Fig. 1). (E) to (H) Clay-rich samples from; channel (E), proximal basin (F), basin 1 (G) and distal basin (H) positions, respectively.

Figure 4: Pairwise Pearson's r correlations between particle shape parameters for clay-poor (A) and clay-rich (B) flows.

Figure 5: Boxplot examples of calculated particle shape parameters for studied clay-poor flow experiments: (A) circularity, (B) roundness, (C) fractal dimension and (D) angularity. Positions within the basin can be seen in Fig. 1. Basin 1, 2 and 3 locations were grouped as 'Basin'. The lowest point is the minimum value of the sample and the highest point is the maximum value of the sample. The box is drawn from Quartile 1 to Quartile 3 (interquartile range) and the horizontal line in the middle represents the median value. The notched part in the box represents a 95% confidence interval for the median value.

Figure 6: Boxplot examples of calculated particle shape parameters for studied clay-rich flow experiments: (A) circularity, (B) roundness, (C) fractal dimension and (D) angularity. Positions within the basin can be seen in Fig. 1. Basin 1, 2 and 3 locations were grouped as 'Basin'. See caption of Fig. 5 for an explanation of boxplot representation.

Figure 7: Boxplot examples of shape variation for a basin cross-flow (oblique) section of the deposit created by F1E5 clay-poor flow experiment. (A) Circularity, (B) roundness, (C) fractal dimension and (D) angularity. Positions within the basin can be seen in Fig. 1. See caption of Fig. 5 for an explanation of boxplot representation.

Figure 8: Boxplot examples of shape variation for a basin cross-flow (strike) section of the deposit created by F2E4 clay-rich flow experiment. (A) Circularity, (B) roundness, (C) fractal dimension and (D) angularity. Positions within the basin can be seen in Fig. 1. See caption of Fig. 5 for an explanation of boxplot representation.

Figure 9: Scatter plots of mean circularity versus mean roundness for samples of (A) Clay-poor flows and (B) clay-rich flows. Position of samples in legend.

Figure 10: Scatter plots of mean circularity versus mean fractal dimension for samples of (A) Clay-poor flows and (B) clay-rich flows. Position of samples in legend.

Figure 11: Scatter plots of mean circularity versus mean solidity for samples of (A) Clay-poor flows and (B) clay-rich flows. Position of samples in legend.

Figure 12: Hierarchical clustering dendrogram for clay-poor flow samples. The appearance of two main clusters (each containing proximally or distally-located samples) can be seen. Flow samples

abbreviations (locations in Fig. 1): Channel (CH), Transition (TR), Proximal Basin (PB), Basin 1 (B1), Basin 2 (B2), Basin 3 (B3), Distal Basin (DB), Basin Margin 1 (BM1), Basin Off-Axis (OA).

Figure 13: Hierarchical clustering dendrogram for clay-rich flow samples. Two sub-clusters (each containing distally-located samples) can be seen which are not connected in the same main cluster, and seem mixed with more proximally-located sub-clusters. Flow samples abbreviations (locations in Fig. 1): Channel (CH), Transition (TR), Proximal Basin (PB), Basin 1 (B1), Basin 2 (B2), Basin 3 (B3), Distal Basin (DB), Basin Margin 1 (BM1), Basin Margin 2 (BM2).

Figure 14: Boxplots of the size of opaque phytoclasts from proximal, medial and distal areas of the Peïra Cava Basin, annotated with typical grain shape in each area. Based on data from McArthur *et al*. (2016b).

Figure 15: General trends of calculated particle shape parameters depending on the position within the experimental basin. The observed trends are clearer for clay-poor, non-cohesive flow experiments.

TABLE CAPTIONS

Table 1: Parameters of conducted flow experiments. Median grain size (D50) was measured from bypass pipe samples using laser diffraction analysis.

Table 2: List of particle image analysis parameters calculated based on Tunwal *et al*. (2018).

Table 3: List of statistical methods and rationale used for analysis of extracted particle shape parameters.

Table 4: Results of Shapiro-Wilk normality testing for distributions of particle shape parameters from all studied flows.

Table 5: Pearson's r correlation coefficients for studied mean shape parameter versus longitudinal distance correlation for all studied flows. Significant correlations (p value < 0.05) in bold numbers. Concentration (vol.%) also shown in brackets for each flow experiment.

Table 6: Best correlated shape parameters for the first two most important principal component analysis (PCA) components, and their cumulative variance for each studied flow experiment.

Flow	Duration (sec)	Volume (l)	Flow Rate (l/min)		Concentration (Vol.%)		Grain-Size Composition (%)				D50 (µm)
			Planned	Observed	Planned	Observed	Clay %	F %	M %	G %	
F1E5	800	400.2	30	30.21	25	21.83	0	56	40	4	65.27
F1E7	800	400.1	30	29.98	10	12.56	0	49	42	8	75.89
F1E11	600	400.6	40	39.85	25	22.90	0	53	38	9	69.40
F1E15	480	402.6	50	48.97	25	20.44	0	40	25	35	56.53
F2E2	800	399.5	30	28.83	30	26.00	34	56	8	2	27.00
F2E3	480	400.1	50	46.52	30	22.00	40	55	4	1	22.00
F2E4	600	401.1	40	38.66	30	29.00	27	51	20	2	37.43

Image analysis parameters	Description
Roundness	Average radius of the circles that are fitted to the corners of the particle divided by the radius of the largest inscribed circle of the particle (Wadell, 1932; Roussillon *et al*., 2009).
Circularity	Square root of the ratio of the diameter of the largest inscribed circle of the particle with the diameter of the smallest circumscribing circle of the particle (Riley, 1941; Blott & Pye, 2008).
Angularity	Average of the five highest differences in angles (after interpolation of particle's boundary as a polygon, Rao *et al*., 2002).
Irregularity	Quantification of the depth of concavities in the particle's boundary with reference to its convex hull (Blott & Pye, 2008).
Fractal Dimension	Measure for particle's boundary roughness (Orford & Whalley, 1983; Hyslip & Vallejo, 1997).
Aspect Ratio	Length of particle's major axis divided by length of minor axis.
Rectangularity	Area of particle divided by area of particle's bounding rectangle.
Compactness	Diameter of circle of equivalent area to particle divided by length of particle's major axis.
Solidity	Particle's area divided by particle's convex area.
Convexity	Particle's convex perimeter divided by perimeter of particle.
Mod Ratio	Diameter of particle's largest inscribed circle divided by particle's feret diameter.

Statistical method	Rationale
Pearson's r correlation/ Normality testing	Investigation of possible correlation between shape parameters and their deviation from a normal (Gaussian) distribution, (Shapiro & Wilk, 1965; Freedman *et al*., 2007).
Boxplots	Investigation of shape parameter variation vs. deposit position within the tank basin.
Shape parameters–Distance correlation	Pearson's linear correlation between mean shape parameters and distance from sediment source.
Principal Component Analysis	Locate important shape parameters that better control data variation (Jolliffe, 2002).
Mean shape parameters scatterplots	Investigate possible trends between samples from different positions.
Kruskal–Wallis and Dunn statistical testing	Detecting important differences between distributions of shape parameters in several locations within the tank basin (Kruskal & Wallis, 1952; Dunn, 1964).
Hierarchical clustering	Detecting clusters of samples based on their mean particle shape parameters (Kaufman & Rousseeuw, 1990).

Flow	Number of Shapiro Wilk Tests Conducted	Number of Shapiro-Wilk Tests With Null Hypothesis Accepted (Normality)	Number of Shapiro-Wilk Tests With Null Hypothesis Rejected (Non-normality)
F1E5	99	16	83
F1E7	77	20	57
F1E11	77	12	65
F1E15	77	14	63
F2E2	77	10	67
F2E3	77	10	67
F2E4	99	14	85

Particle Shape Parameter	Clay-Poor Flows (Pearson's r , Shape Parameter-Longitudinal Distance)				Clay-Rich Flows (Pearson's r , Shape Parameter-Longitudinal Distance)		
	F1E5 (21.8%)	F1E7 (12.5%)	F1E11 (22.9%)	F1E15 (20.4%)	F2E2 (26%)	F2E3 (22%)	F2E4 (29%)
Roundness	0.02	**0.78**	0.38	0.32	- 0.66	- 0.50	0.49
Circularity	**- 0.96**	**- 0.87**	**- 0.81**	**- 0.84**	- 0.73	- 0.38	- 0.62
Angularity	0.74	**0.88**	-0.10	- 0.16	0.08	**- 0.80**	0.16
Irregularity	**0.81**	**0.82**	0.59	**0.83**	0.52	0.01	0.34
Fractal Dimension	**0.89**	**0.80**	0.57	0.65	0.62	- 0.74	0.59
Aspect Ratio	**0.93**	**0.91**	**0.84**	**0.87**	**0.75**	0.53	0.42
Rectangularity	**- 0.77**	**- 0.88**	-0.37	- 0.62	- 0.02	0.30	- 0.35
Compactness	**- 0.96**	**- 0.83**	**- 0.83**	**- 0.83**	- 0.70	- 0.51	- 0.57
Solidity	**- 0.92**	**- 0.79**	- 0.61	**- 0.86**	- 0.44	0.34	- 0.43
Convexity	0.23	**0.83**	- 0.10	- 0.11	0.62	0.36	0.15
Mod Ratio	**- 0.95**	**- 0.88**	**- 0.79**	**- 0.85**	- 0.72	- 0.30	- 0.61

Flow	Principal Component 1 Better Correlated Shape Parameter	Principal Component 2 Better Correlated Shape Parameter	Cumulative Proportion of Variance
F1E5	Circularity	Fractal Dimension	62.8%
F1E7	Circularity	Fractal Dimension	63.5%
F1E11	Mod Ratio	Roundness	64.2%
F1E15	Mod Ratio	Roundness	64.3%
F2E2	Circularity	Roundness	63.7%
F2E3	Circularity	Roundness	64.8%
F2E4	Circularity	Roundness	65.0%

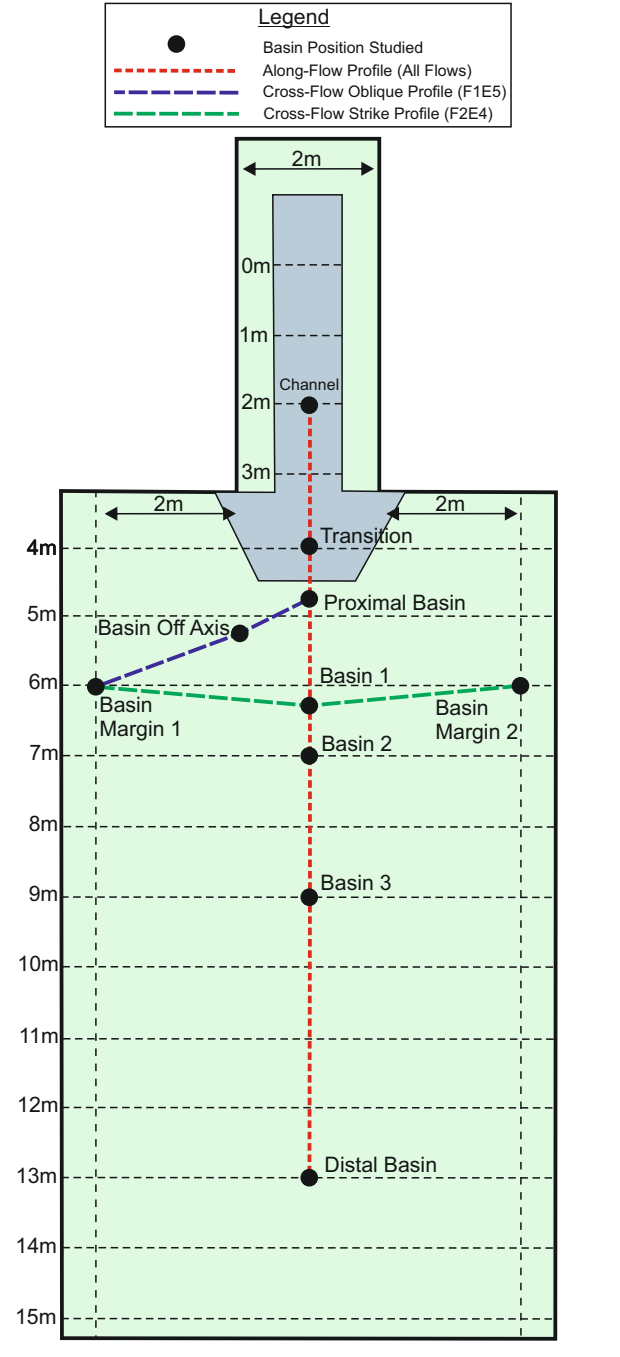
Legend
Basin Position Studied
Along-Flow Profile (All Flows)
Cross-Flow Oblique Profile (F1E5)
Cross-Flow Strike Profile (F2E4)
2m
0m
1m
Channel
2m
3m
2m
2m
4m
Transition
5m
Proximal Basin
Basin Off Axis
6m
Basin 1
Basin
Margin 1
Basin
Margin 2
7m
Basin 2
8m
9m
Basin 3
10m
11m
12m
13m
Distal Basin
14m
15m


A


B

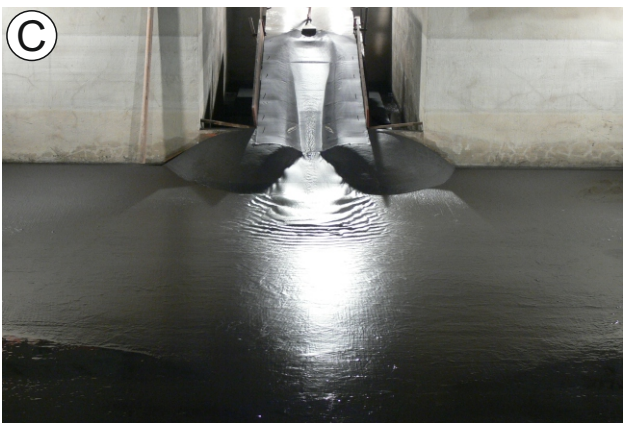
C

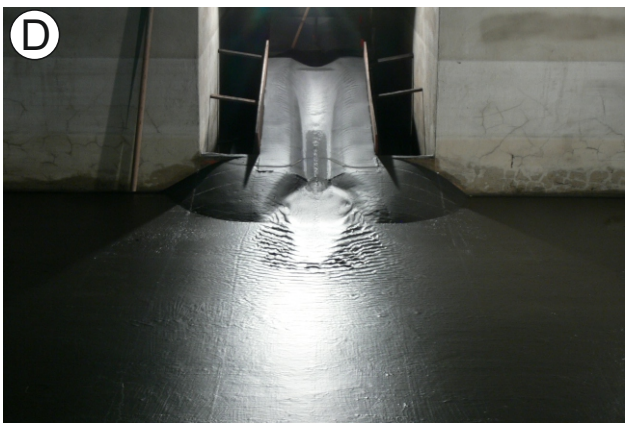
D


E

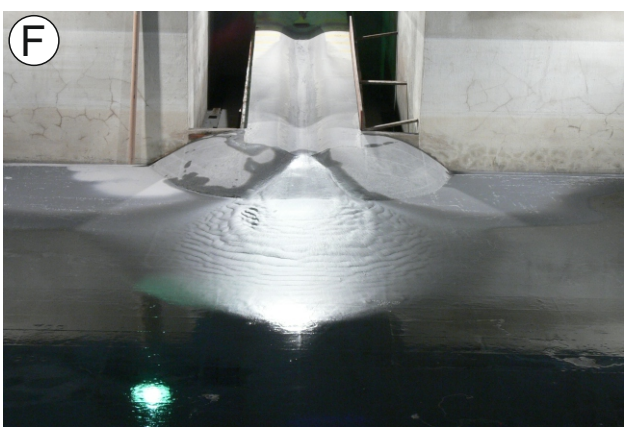
F


G

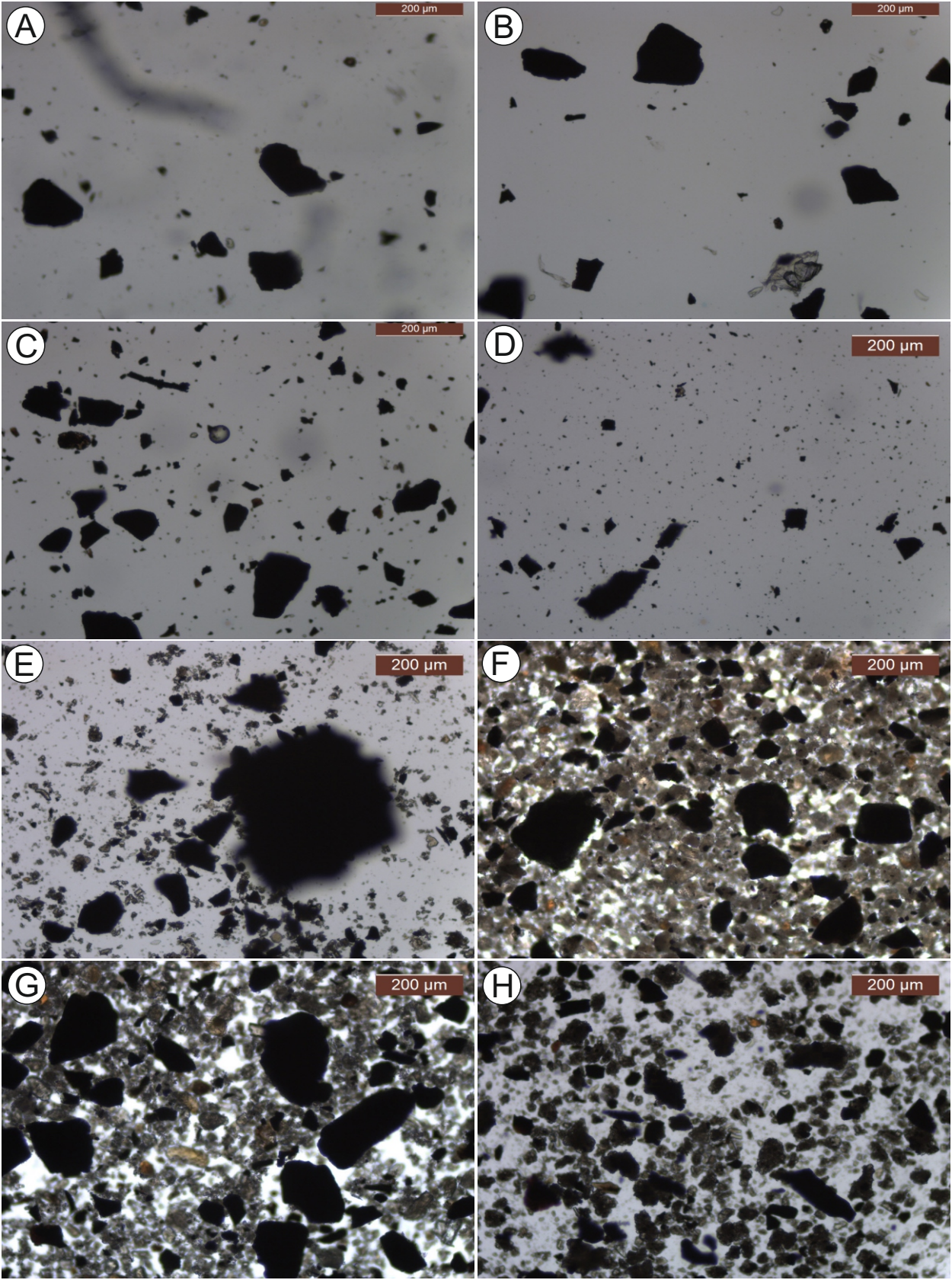
A
200 µm
B
200 µm
C
200 µm
D
200 µm
E
200 µm
F
200 µm
G
200 µm
H
200 µm

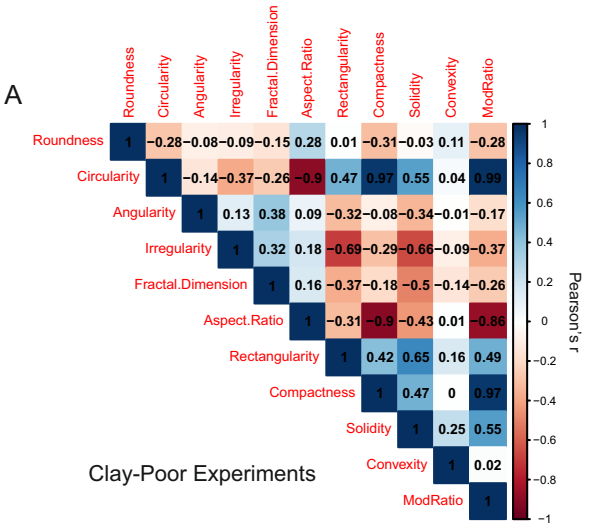
A
Roundness
Circularity
Angularity
Irregularity
Fractal.Dimension
Aspect.Ratio
Rectangularity
Compactness
Solidity
Convexity
ModRatio
1 -0.28 -0.08 -0.09 -0.15 0.28 0.01 -0.31 -0.03 0.11 -0.28
1 -0.14 -0.37 -0.26 -0.9 0.47 0.97 0.55 0.04 0.99
1 0.13 0.38 0.09 -0.32 -0.08 -0.34 -0.01 -0.17
1 0.32 0.18 -0.69 -0.29 -0.66 -0.09 -0.37
1 0.16 -0.37 -0.18 -0.5 -0.14 -0.26
1 -0.31 -0.9 -0.43 0.01 -0.86
1 0.42 0.65 0.16 0.49
1 0.47 0 0.97
1 0.25 0.55
1 0.02
1
Pearson's r
1
0.8
0.6
0.4
0.2
0
-0.2
-0.4
-0.6
-0.8
-1
Clay-Poor Experiments
B
Roundness
Circularity
Angularity
Irregularity
Fractal.Dimension
Aspect.Ratio
Rectangularity
Compactness
Solidity
Convexity
ModRatio
1 -0.29 -0.14 -0.16 -0.16 0.36 0.07 -0.32 -0.03 0.08 -0.28
1 -0.19 -0.36 -0.28 -0.89 0.45 0.97 0.55 0.01 0.99
1 0.18 0.42 0.13 -0.32 -0.13 -0.36 -0.01 -0.21
1 0.36 0.2 -0.7 -0.28 -0.67 -0.1 -0.35
1 0.22 -0.37 -0.21 -0.5 -0.07 -0.27
1 -0.3 -0.89 -0.46 0.05 -0.84
1 0.4 0.63 0.23 0.45
1 0.49 -0.01 0.97
1 0.23 0.54
1 0
1
Pearson's r
1
0.8
0.6
0.4
0.2
0
-0.2
-0.4
-0.6
-0.8
-1
Clay-Rich Experiments

Along-Flow Profile

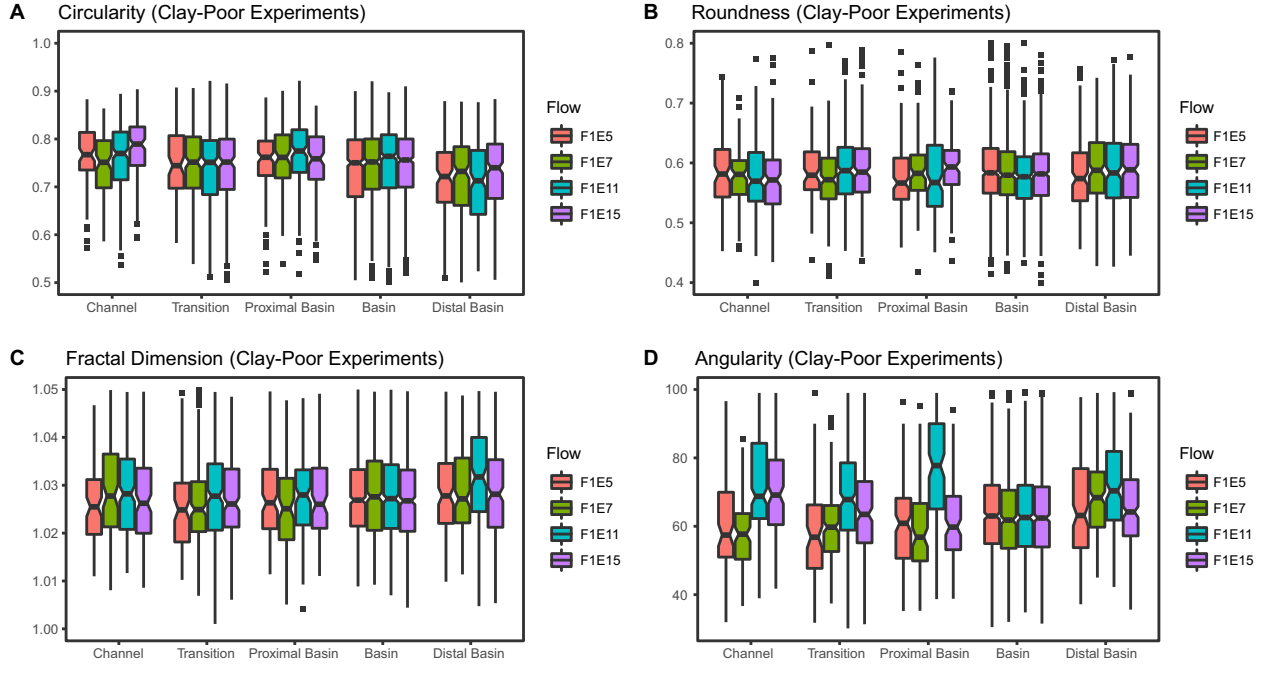

Along-Flow Profile

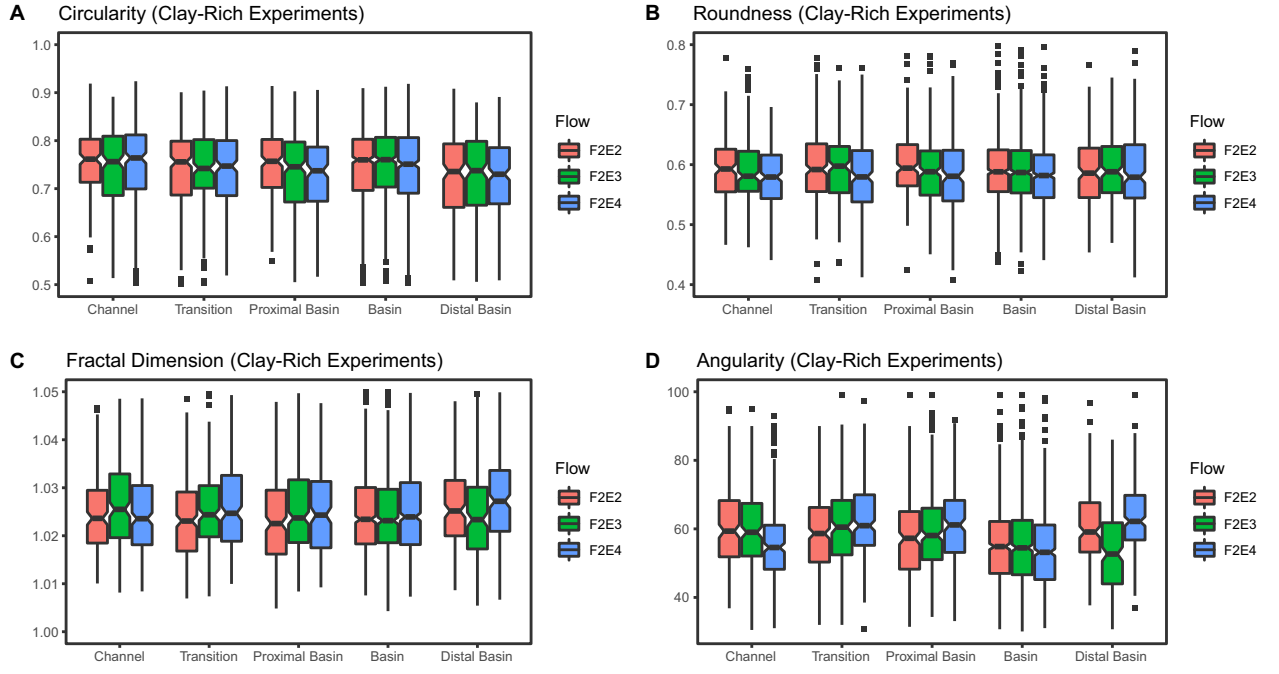

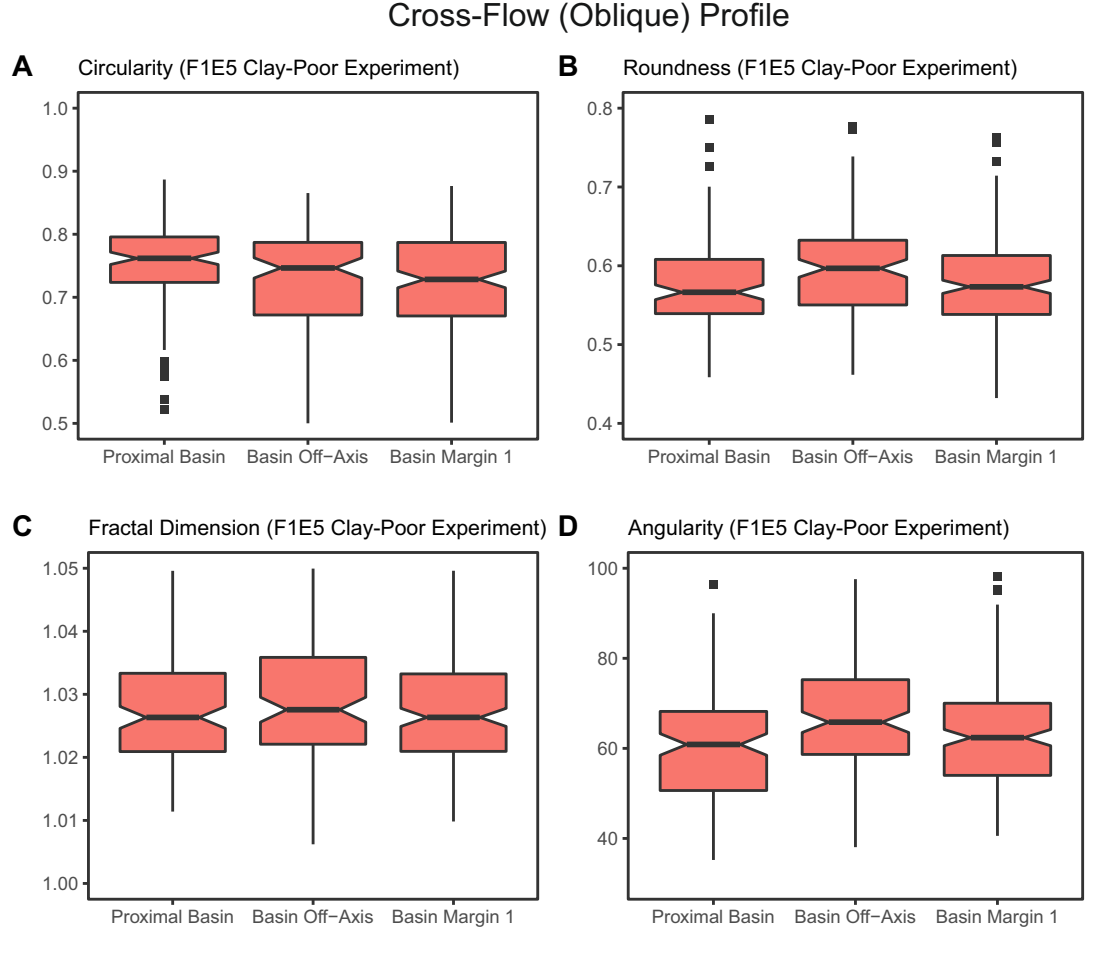
Cross-Flow (Oblique) Profile
A
Circularity (F1E5 Clay-Poor Experiment)
1.0
0.9
0.8
0.7
0.6
0.5
Proximal Basin
Basin Off−Axis
Basin Margin 1
B
Roundness (F1E5 Clay-Poor Experiment)
0.8
0.7
0.6
0.5
0.4
Proximal Basin
Basin Off−Axis
Basin Margin 1
C
Fractal Dimension (F1E5 Clay-Poor Experiment)
1.05
1.04
1.03
1.02
1.01
1.00
Proximal Basin
Basin Off−Axis
Basin Margin 1
D
Angularity (F1E5 Clay-Poor Experiment)
100
80
60
40
Proximal Basin
Basin Off−Axis
Basin Margin 1

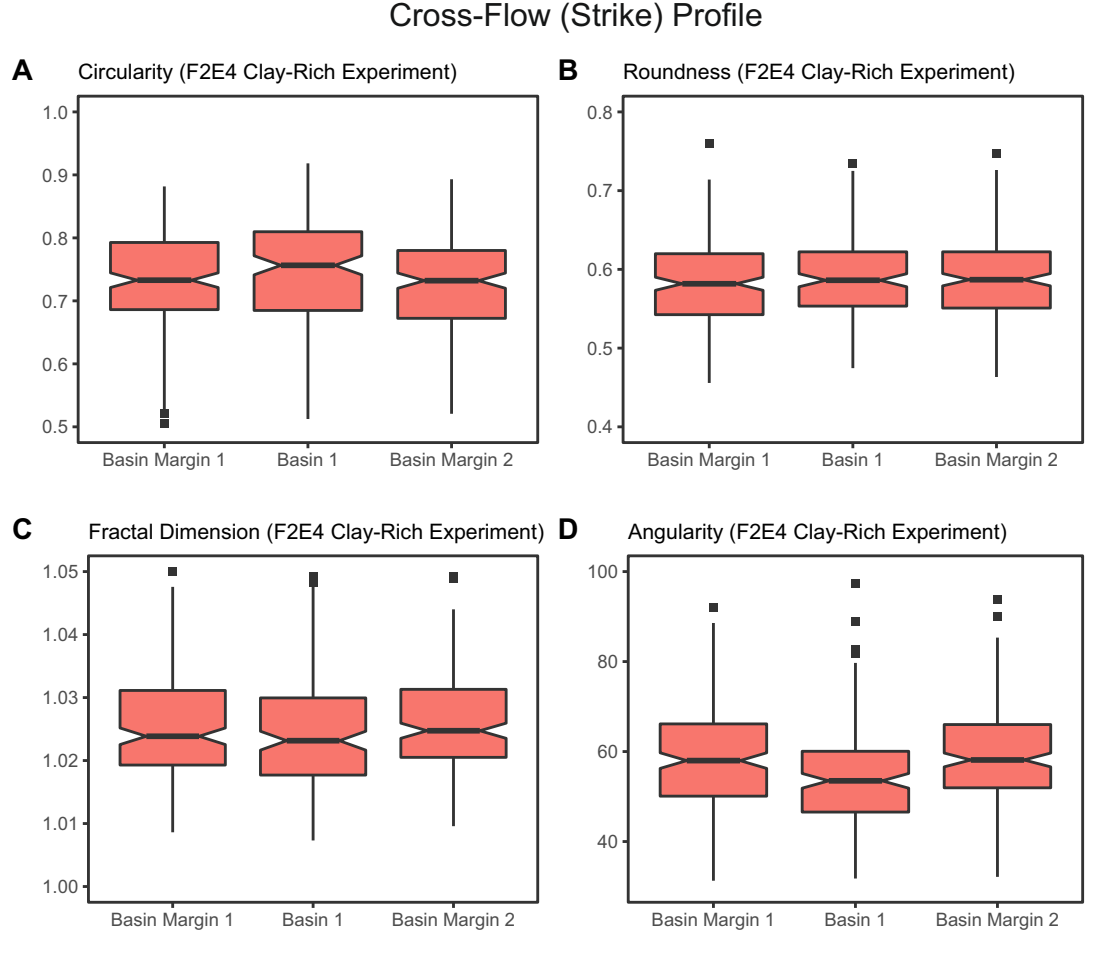
Cross-Flow (Strike) Profile
A
Circularity (F2E4 Clay-Rich Experiment)
1.0
0.9
0.8
0.7
0.6
0.5
Basin Margin 1
Basin 1
Basin Margin 2
B
Roundness (F2E4 Clay-Rich Experiment)
0.8
0.7
0.6
0.5
0.4
Basin Margin 1
Basin 1
Basin Margin 2
C
Fractal Dimension (F2E4 Clay-Rich Experiment)
1.05
1.04
1.03
1.02
1.01
1.00
Basin Margin 1
Basin 1
Basin Margin 2
D
Angularity (F2E4 Clay-Rich Experiment)
100
80
60
40
Basin Margin 1
Basin 1
Basin Margin 2

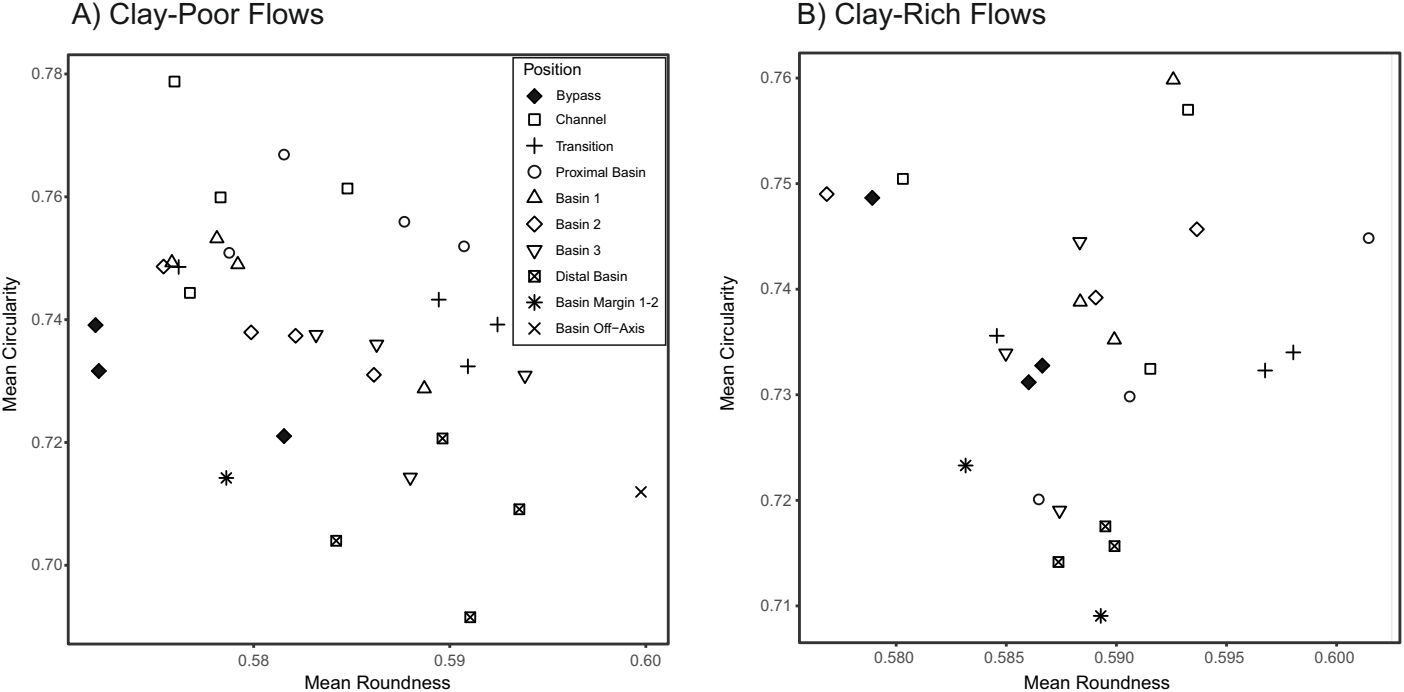
A) Clay-Poor Flows
B) Clay-Rich Flows
Position
Bypass
Channel
Transition
Proximal Basin
Basin 1
Basin 2
Basin 3
Distal Basin
Basin Margin 1-2
Basin Off−Axis
Mean Circularity
Mean Roundness
0.78
0.76
0.74
0.72
0.70
0.58
0.59
0.60
0.76
0.75
0.74
0.73
0.72
0.71
0.580
0.585
0.590
0.595
0.600

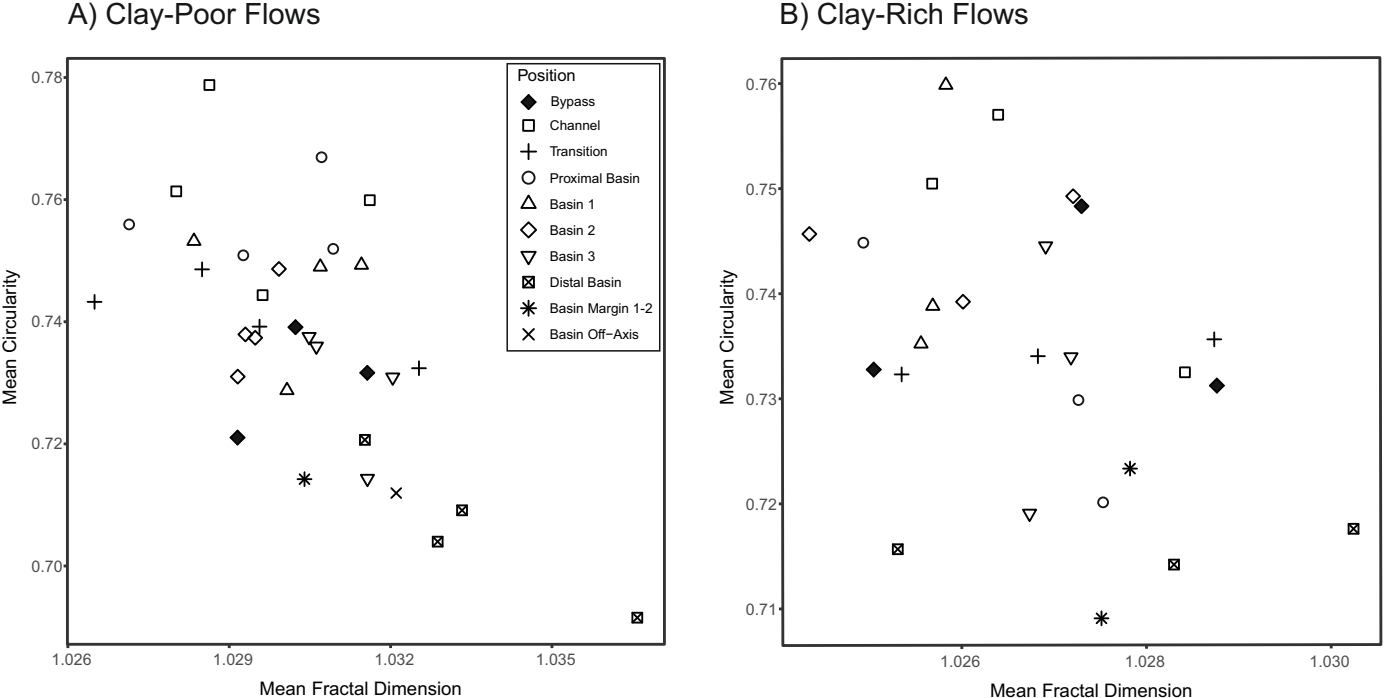
A) Clay-Poor Flows
B) Clay-Rich Flows
Position
Bypass
Channel
Transition
Proximal Basin
Basin 1
Basin 2
Basin 3
Distal Basin
Basin Margin 1-2
Basin Off−Axis
Mean Circularity
Mean Fractal Dimension
0.78
0.76
0.74
0.72
0.70
1.026
1.029
1.032
1.035
0.76
0.75
0.74
0.73
0.72
0.71
1.026
1.028
1.030

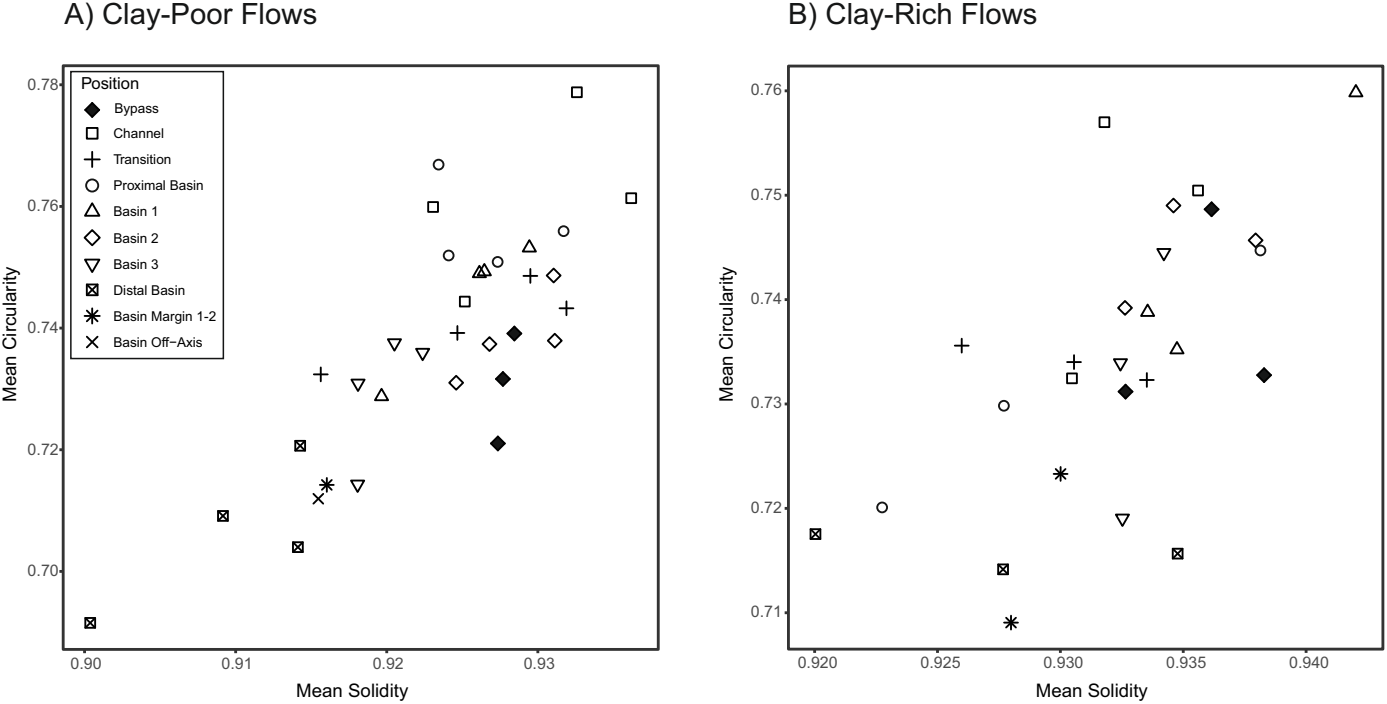
A) Clay-Poor Flows
B) Clay-Rich Flows
Position
Bypass
Channel
Transition
Proximal Basin
Basin 1
Basin 2
Basin 3
Distal Basin
Basin Margin 1-2
Basin Off−Axis
Mean Circularity
Mean Solidity
0.78
0.76
0.74
0.72
0.70
0.90
0.91
0.92
0.93
0.76
0.75
0.74
0.73
0.72
0.71
0.920
0.925
0.930
0.935
0.940

Clay-Poor Flows
Hierarchical Clustering
(Euclidean Distance, Ward Method)

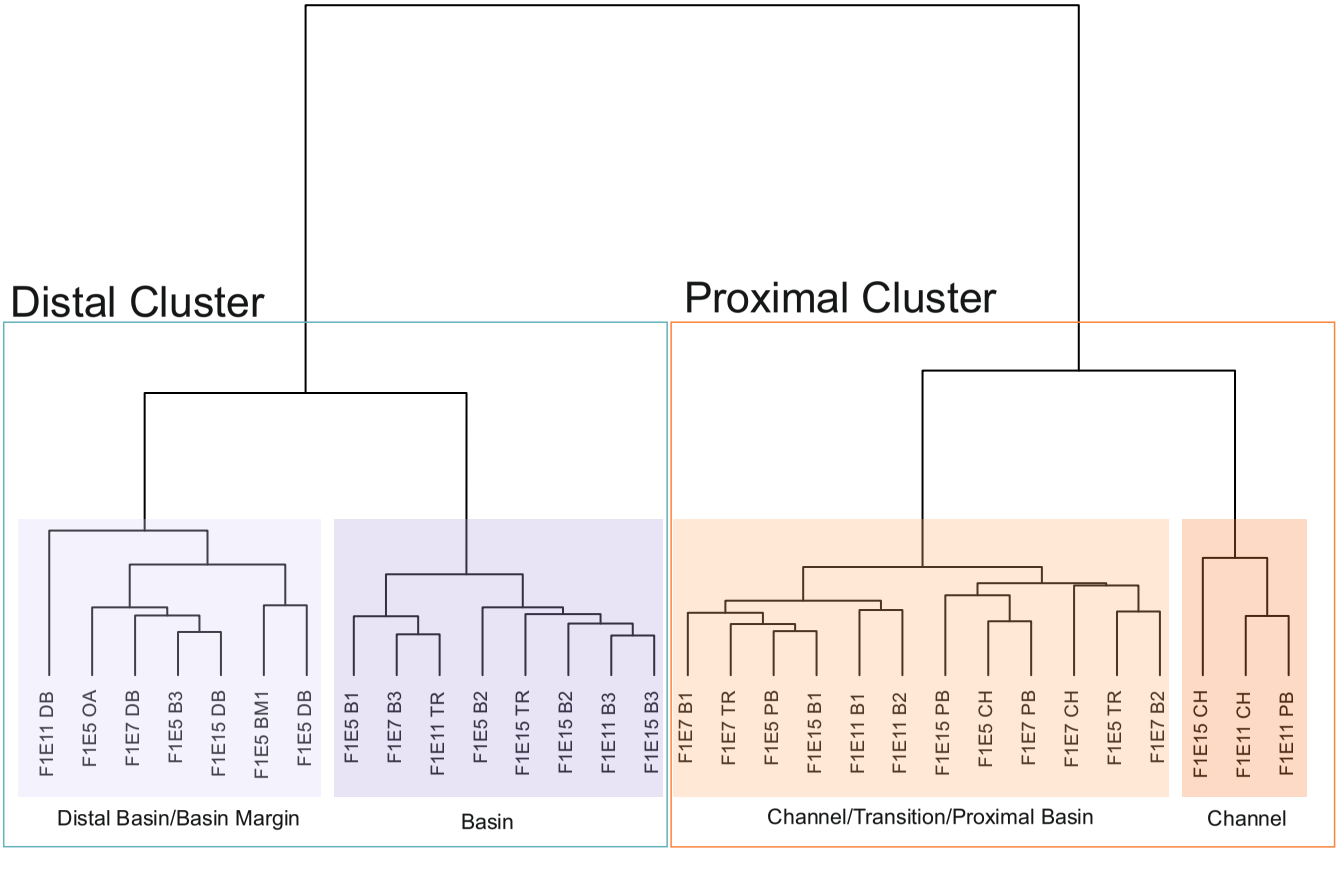

Clay-Rich Flows
Hierarchical Clustering
(Euclidean Distance, Ward Method)

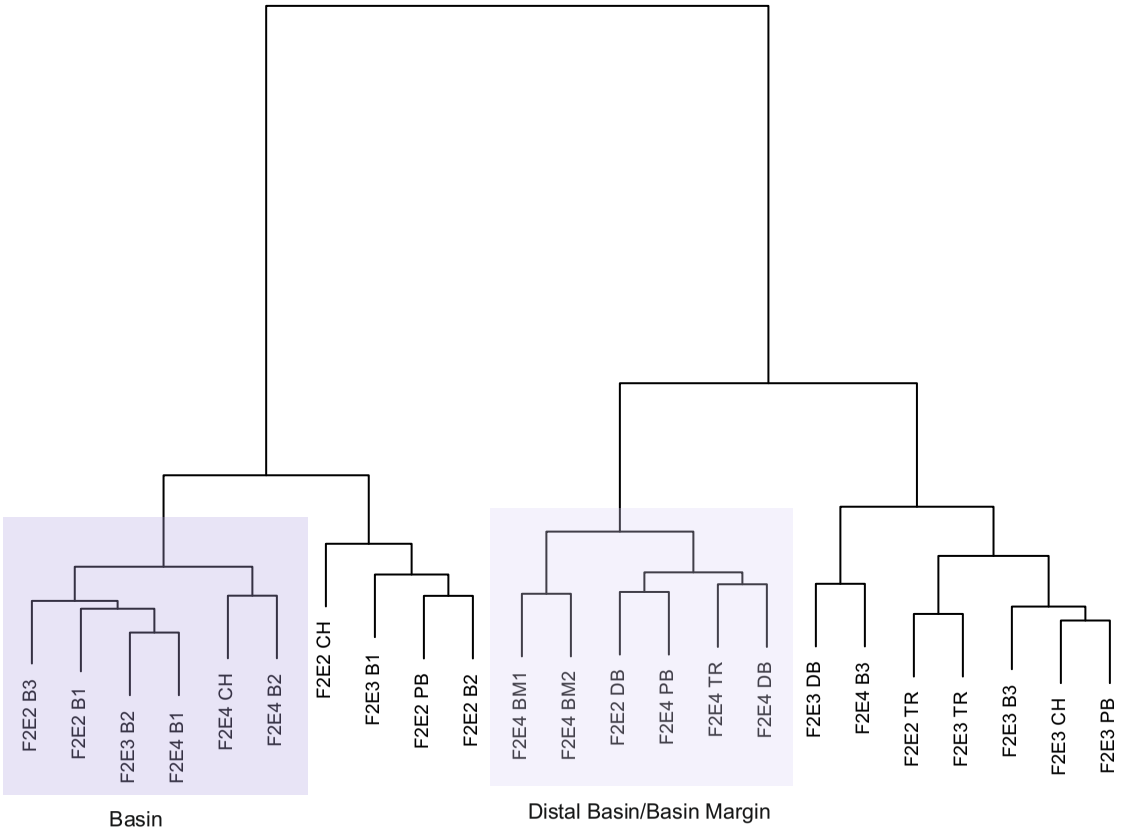

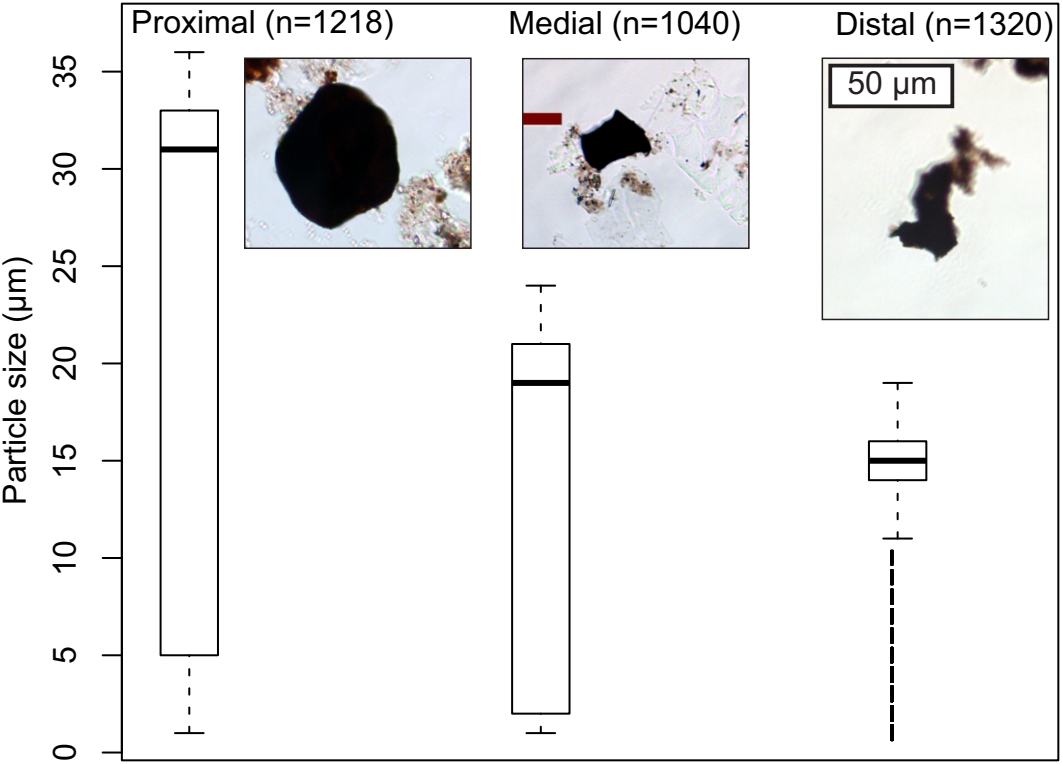
Proximal (n=1218)
Medial (n=1040)
Distal (n=1320)
50 µm
Particle size (µm)
0
5
10
15
20
25
30
35

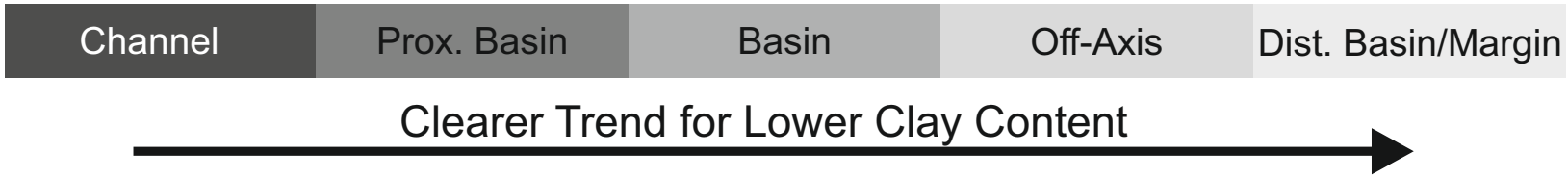

Increase	Aspect Ratio, Fractal Dimension, Roundness, Irregularity
Decrease	Circularity, Compactness, Mod Ratio, Solidity, Rectangularity
No Trend	Angularity, Convexity